

Monitoring the Material Quality of Two-Dimensional Transition Metal Dichalcogenides

Jinhuan Wang, Chen Huang, Yilong You, Quanlin Guo, Guodong Xue, Hao Hong, Qingze Jiao, Dapeng Yu, Lena Du,* Yun Zhao,* and Kaihui Liu*



Cite This: <https://doi.org/10.1021/acs.jpcc.2c00051>



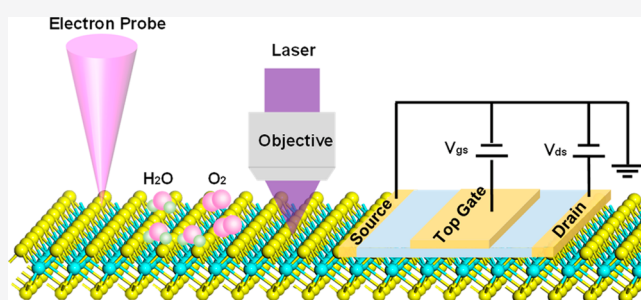
Read Online

ACCESS |

Metrics & More

Article Recommendations

ABSTRACT: Two-dimensional (2D) transition metal dichalcogenides (TMDs), with atomic thickness, strong spin–orbit coupling, enhanced light–matter interactions, and facile quantum control ability, have demonstrated great potential in the applications of nanoelectronics and optoelectronics. The realization of these high-performance applications strongly relies on the production of large-scale TMD films with high quality. Therefore, facile and accurate quality monitoring of TMDs is essential for their future applications. In this Review, we summarized the main defect types in TMD crystals obtained by different synthesis methods, and we discussed recent cutting-edge characterization techniques, including scanning transmission electron microscopy, transistors. Finally, we provide a short perspective on the future materials.



etching or adsorption, optical spectroscopy, and field-effect development of quality monitoring techniques for broad 2D

1. INTRODUCTION

Two-dimensional (2D) transition metal dichalcogenides (TMDs) are representative layered inorganic semiconductors with the formula MX_2 , where M is a transition metal atom (e.g., Mo and W), and X is a chalcogen atom (S, Se, or Te). The M atom is covalently sandwiched between two X atoms forming a hexagonal honeycomb lattice structure in a single layer, and adjacent layers interact via weak van der Waals forces.¹ In 1963, an ultrathin single-crystal MoS_2 was obtained for the first time by peeling from a large crystal of MoS_2 .² Subsequently, in 1986, monolayer MoS_2 was exfoliated by intercalation with lithium and reaction with water.³ However, it was not until monolayer graphene was obtained in 2004⁴ that TMDs began to be intensively investigated. In contrast to the gapless semimetal graphene, TMDs possess direct energy band gaps in the near-infrared to visible spectral region at the two inequivalent K and K' momentum valleys in the Brillouin zone.^{5–13} Due to strong spin–orbit interactions, these two valleys couple to the electron spin and exhibit valley-selective light interactions.^{14–18} Such novel electronic structures make TMDs promising for an enormous range of advanced applications in lasers,^{19–23} memory devices,^{24–29} photo-detectors^{30–36} and extremely thin channel transistors.^{37–41}

High-performance applications of TMDs are guaranteed by the production of high-quality material. In terms of sample preparation, 2D TMDs can be synthesized through top-down methods, including mechanical exfoliation (ME)^{42–49} and

liquid phase exfoliation,^{50–52} and bottom-up methods mainly including molecular beam epitaxy (MBE)^{53–57} and chemical vapor deposition (CVD).^{58–63} However, due to the 2D nature and ultrahigh specific surface areas of TMDs, it is impossible to avoid introducing defects during sample synthesis with any method.^{64,65} These lattice defects can be divided into two main types: point defects in individual island and grain boundaries (GBs) between two stitched islands.^{66–71} Different from that of the single-element materials (such as graphene), the formation of point defects in TMDs is mainly due to the insufficient supply of the transition metal or the chalcogen precursor, as it is particularly difficult to precisely control these two compounds. GBs in polycrystalline TMDs result from the stitching of grains with random grain orientations during the growth.

The presence of defects significantly influences the intrinsic properties of 2D TMDs.^{72–79} Those defects acting as scattering centers introduce strongly localized midgap states in the electronic structure, which may result in failing to open new transport channels and reduce the mobility of charge

Received: January 4, 2022

Revised: February 11, 2022

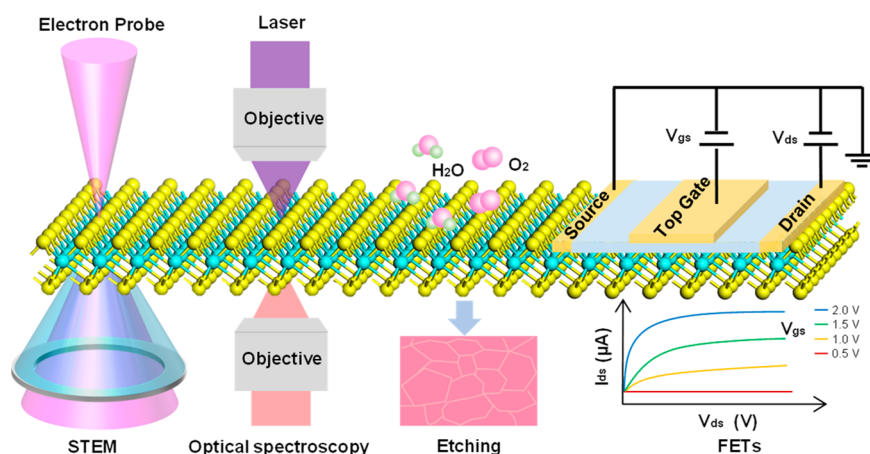


Figure 1. Schematic illustration of four key aspects for the quality characterization of TMDs.

carriers through the intrinsic conduction or valence band.⁸⁰ Defects will bring in more nonradiative recombination channels in TMDs, and thus reduce the exciton lifetime and PL quantum yield.⁸¹ While, those defects can also bring many exotic applications. For example, the trapped exciton by defects in TMDs can be an ideal sources of single photon emitters.⁸² Defects in TMDs can serve as new catalytic sites used to promote hydrogen evolution reactions.^{83–86} Hence, building a standard set of defect characterization techniques for systematically monitoring the material quality of TMDs is a prerequisite for real application of these materials.

For the material quality monitoring of traditional semiconductors (e.g., silicon, germanium, and gallium arsenide), a series of national standards have been established. For example, the crystallization defects of silicon can be identified by the chemically preferential etching techniques, and the contents of substitutional carbon and interstitial oxygen can be monitored by infrared absorption spectroscopy. Furthermore, the monitoring of electrical performances such as the resistivity, conductivity type, and minority carrier lifetime have formulated standardized methods to meet quality requirements. Nevertheless, unlike traditional bulk semiconductor materials, where defects and impurities are embedded inside the crystal, the particularity of 2D materials limits the distribution of all defects on the surface of the material. This intrinsic feature provides a unique opportunity to detect defects in 2D materials by different means of surface sciences.

In this review, we considered the defects in TMDs in detail and summarized four key quality characterization (the characterization of defects) techniques (Figure 1): namely, atomic-scale characterization by scanning transmission electron microscopy (STEM); defect visualization by etching or adsorption; high-throughput characterization by optical spectroscopy such as Raman spectroscopy, second harmonic generation (SHG), and photoluminescence (PL); and electrical transport measurement by field-effect transistors (FETs). The accurate monitoring and comprehensive understanding of defects in TMDs are of great importance for the improvement of TMD quality and the realization of superior behaviors in their potential applications.

2. QUALITY CHARACTERIZATION TECHNIQUES FOR TMDs

2.1. Atomic-Scale Characterization by STEM.

As an indispensable component of materials science, microscopy and microanalysis are important methods to practice “seeing is believing” and to explore the microscopic world. In recent years, the development of spherical aberration correction technology has further improved the spatial resolution of transmission electron microscopy (TEM), enabling the imaging of individual atoms. Benefiting from this, high-resolution TEM (HRTEM) and STEM are common techniques for characterizing the atomic structure of 2D TMDs. With these techniques, the structures of defects in TMDs can be directly observed.^{87,88} Different from the isotropy of 3D crystal structure, 2D TMDs possess layered structure with atomically thin thickness. As STEM delivers the projection of the sample along with the beam direction, ultimate thickness of TMDs facilitate the identify of atomic position. In contrast, the atomically precise characterization of 3D atomic structures remains difficult.

HRTEM is an imaging technique based on phase contrast that enables direct observation of the atomic structure of a sample. The defects can be clearly distinguished by analyzing the intensity profile in the HRTEM images.^{89–91} However, the HRTEM technique usually delivers lattice images rather than real atomic images. In contrast, the STEM technique has the ability to provide incoherent atomic images, whose intensity directly corresponds to the atomic number (*Z*-contrast). Namely, atoms can be distinguished by their brightness, making STEM technique more suitable for the comprehensive and systematic study of defective atomic structures in TMDs.^{92–95} Notably, since electron beam irradiation brings irreversible damage to TMDs, low voltage TEM imaging (~80 kV) is commonly used in TMDs.

With the aid of STEM technique, intrinsic structural defects in TMDs can be classified into two categories according to their dimensionality: zero-dimensional (point) and one-dimensional (line) defects. Regardless of foreign atoms, there are two kinds of predominant point defects in TMDs: vacancies as a result of losing the M atom, X atom, MX₃, or MX₆, and antisite defects in which M (X) atoms substitute for X (M) atoms. The most common vacancies in TMDs are the loss of chalcogen atoms. In monolayer MoS₂, the representative vacancies are monosulfur vacancies (V_S) and disulfur vacancies (V_{S2}) (Figure 2a, left), and common antisite defects

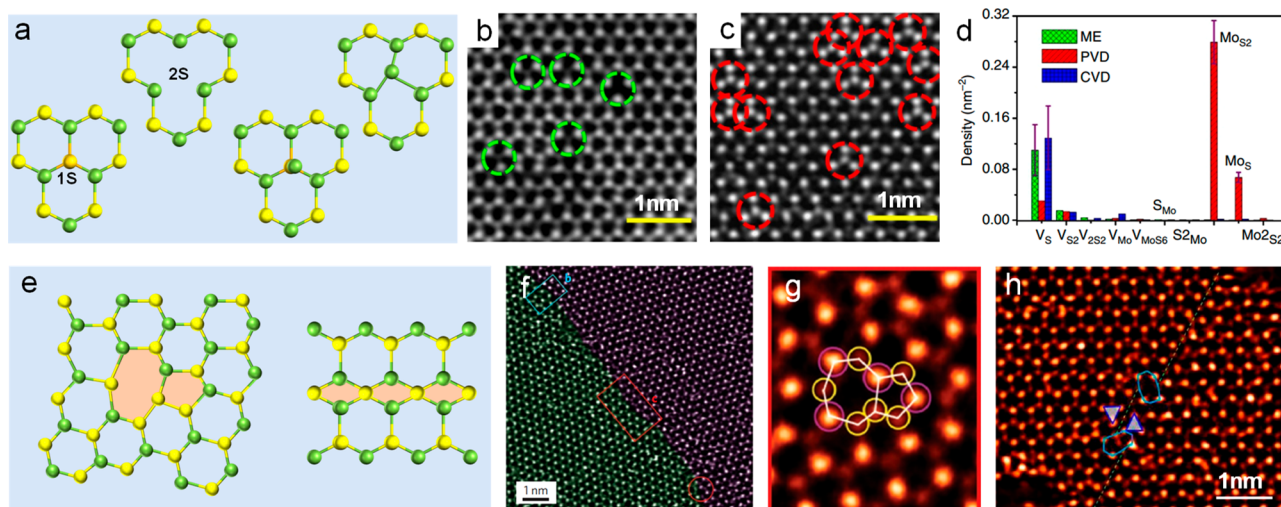


Figure 2. Atomic-scale characterization of defects in TMDs by STEM. (a) Atomic models of point defects, including V_S , V_{S_2} , Mo_S , and Mo_{S_2} . Key: green, Mo atoms; gold, S atoms. (b) Atomic resolution STEM images of V_S and V_{S_2} . (c) Atomic resolution STEM images of Mo_S and Mo_{S_2} . (d) Histogram of various point defects in PVD, CVD and ME monolayers. ME data are in green, PVD data in red and CVD in blue. (b–d) reproduced with permission from ref 97. Copyright 2015 The Author(s). (e) Atomic model of 5/7 fold rings and 4/4 fold rings in GBs. (f) STEM-ADF image of a MoS_2 GB with its dislocations highlighted. (g) Zoom-in image of the region highlighted in part f. The purple circles are Mo and yellow ones are S_2 columns. Parts f and g) were reproduced with permission from ref 105. Copyright 2013 Nature Publishing Group. (h) 4/4P 60° grain boundary. Reproduced with permission from ref 96. Copyright 2013 American Chemical Society.

involve Mo atoms substituting for S atoms, including Mo_S and Mo_{S_2} (Figure 2a, right). Statistics based on STEM images show that the dominant type of point defects in MoS_2 highly depends on the specific synthesis method (Figure 2b–d).^{96,97} Sulfur vacancies are the predominant point defects in mechanical exfoliated and CVD-grown samples, while antisite defects represented by Mo_S and Mo_{S_2} are dominant in the samples deposited by physical vapor deposition (PVD). Therefore, the statistics of point defect density determined from STEM images are of great significance to the quality evaluation of TMDs.^{98–100} Single vacancies are mobile under electron irradiation and tend to agglomerate into line defects due to the low migration barrier.^{101–103} Interestingly, the band structure gradually shifts from semiconducting to metallic as these line defects increase in width.¹⁰⁴

As the most common line defect, a tilt GB is formed when two TMD grains with a lattice orientation mismatch are atomically stitched together with dislocation cores. These dislocation cores in GBs are composed of 5- and 7-fold (5/7) rings (Figure 2e, left), 4/6 fold rings, and 6/8 fold rings due to substitutions between metal and chalcogen atoms.^{91,105} GBs in MoS_2 with atomic configurations of dislocation cores can be visually observed by STEM (Figure 2f).¹⁰⁵ The Mo-oriented dislocation consists of 5/7-fold rings. One of five distinct Mo sites is energetically preferable for substitution by S_2 , forming the most stable structure (Figure 2g). In addition, mirror twin boundaries are observed by STEM when two domains with opposite lattice orientations (60° or 180°) in TMDs are spliced together (Figure 2h).^{96,106} They are composed of 4-fold rings, adopting a 4/4P type (Figure 2e right) and 4/4E type structures.¹⁰⁷

The HRTEM and STEM can provide accurate information on the defect structure with atomic-level spatial resolution, but both fail to characterize large-scale materials. Moreover, the sample must be transferred to a specific microgrid before being characterized.

In addition to the TEM techniques mentioned above, scanning tunneling microscopy (STM) can also be used to characterize the atomic structure of TMDs. Compared with TEM and STEM, STM is superior in characterizing point defects in MoS_2 ¹⁰⁸ and Moiré fringes¹⁰⁹ instead of line defects. At the same time, STM has the advantage of revealing the electronic properties influenced by point defects.^{110,111} However, STM is limited by the sample circumstances, failing for samples grown on insulating substrates.

Atomic force microscopy (AFM) is also a powerful method with high resolution at atomic level invented after STM. In contrast to STM, AFM provides a true three-dimensional view of the surface and does not require any special treatment of the sample. The defect structure in monolayer WS_2 has been detected by the CO-tip noncontact AFM.¹¹² Nevertheless, AFM is restricted to the scanning range and speed.

2.2. Defect Visualization by Etching or Adsorption.

Compared with atomic characterizations tools, simple, effective, and fast methods for defect visualization of large-area TMDs are still lacking. In this view, conventional optical microscopy is an appealing technique to achieve macroscale characterization. However, it is challenging in recognizing ambiguous GBs due to its weak optical contrast. Based on the selective etching and controlled adsorption, the optical contrast of defects could be greatly increased, thus achieving defect visualization of TMDs in a large area.

Mild oxidation under moisture-rich ambient conditions is introduced to visualize GBs in WS_2 domains by scanning electron microscope.¹¹³ However, the side effects of oxidation increase the number of defects in the whole crystalline domains, easily resulting in the PL intensity quenching effect. The key parameters in this experiment were heating temperature and humidity. Therefore, GBs in WS_2 domains through controlled heating in air can be observed by an optical microscope.¹¹⁴ In addition, UV irradiation under moisture-rich air can generate oxygen and hydroxyl radicals, which can selectively functionalize GBs in WSe_2 to provoke morpho-

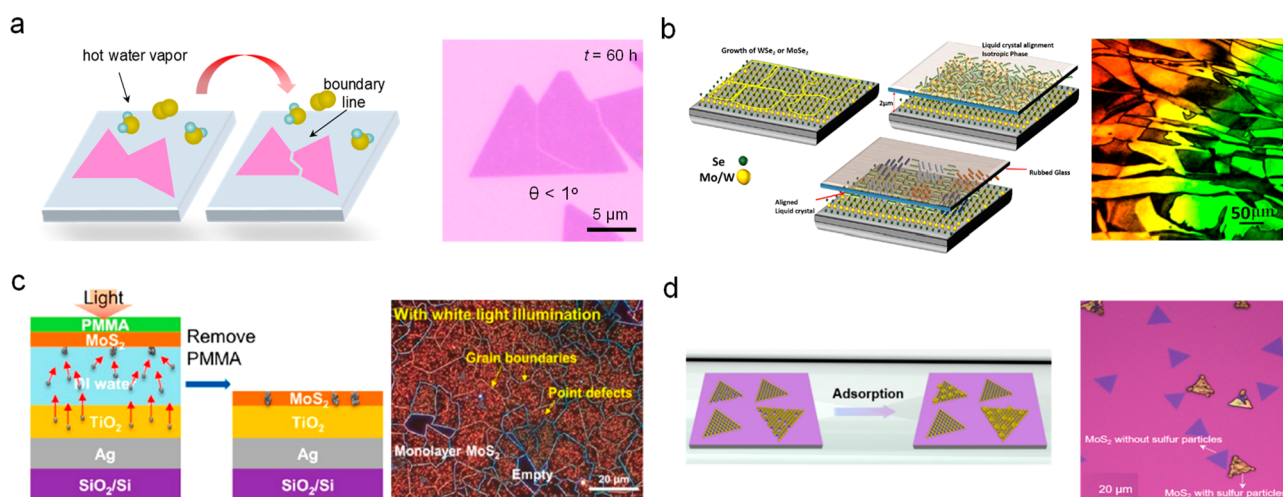


Figure 3. Visualizing defects in TMDs by etching or adsorption. (a) Schematic for mild H_2O vapor-assisted TMDs visualizing all types of grain boundaries unambiguously by optical microscopy. Reproduced with permission from ref 117. Copyright 2018 Tsinghua University Press and Springer-Verlag GmbH Germany. (b) Schematics showing the different grains with different colors when LC molecules were coated on a 2D surface via polarized microscopy. Reproduced with permission from ref 118. Copyright 2017 American Chemical Society. (c) Schematic illustration of preparing a simple $\text{TiO}_2/\text{Ag}/\text{SiO}_2/\text{Si}$ substrate to visualize the point defect distribution of monolayer TMDs using dark-field optical microscopy. Reproduced with permission from ref 119. Copyright 2016 American Chemical Society. (d) Schematic of one-pot selective adsorption of sulfur particles directly on as-synthesized MoS_2 monolayers for rapid and large-scale quality assessment by optical visualization. Reproduced with permission from ref 122. Copyright 2021 American Chemical Society.

logical changes at the GBs.¹¹⁵ However, the PL spectral intensity at 756 nm decreases significantly after oxidation. The MoS_2 films on a SiO_2/Si substrate are exposed to vapor hydrofluoric acid (VHF) for 30–120 s, allowing GB visualization by optical microscopy.¹¹⁶ Nevertheless, this method is invasive for TMD films. Furthermore, a high-throughput method using mild hot H_2O enables visualization of all types of GBs unambiguously in TMD films under an optical microscope, which is nearly noninvasive to the TMD grain domains (Figure 3a).¹¹⁷

Furthermore, discriminative adsorption behaviors among crystalline TMD films have been demonstrated to be a facile approach for detecting defects. The spin-coated liquid crystal (LC) molecules on the surface of the samples have a higher adsorption energy along the armchair direction, thus forcing them to align parallelly to this direction. Such alignment enables the visualization of GBs in CVD-grown MoSe_2 and WSe_2 films by the polarized microscopy (Figure 3b).¹¹⁸ As organic molecules cannot be desorbed clearly, this method greatly damages the quality of TMD films. Furthermore, GBs and point defects can be simultaneously visualized under dark-field optical microscopy, which is realized by anchoring silver nanoparticles on defect sites of MoS_2 under light illumination (Figure 3c).¹¹⁹ The point defect density can be estimated from the population of Ag particles, however, which also suffer from the destruction on the surface of TMD materials. The defects on 2D TMDs possess high reactivities due to the unsaturated chemical bonds, which enables spontaneous anchoring of metal atoms and clusters through redox or coordination.^{120,121}

Recently, a noninvasive method by one-pot adsorption of abundant sulfur particles on CVD-grown MoS_2 monolayers is developed to directly assess the crystal quality based on the preferential adsorption of domains with sulfur vacancies (Figure 3d).¹²² Importantly, the sample surfaces could be recovered after a mild annealing process.

Achieving simple, effective, and noninvasive defect visualization in large-scale TMDs by conventional optical micros-

copy is indispensable to assess the quality of TMDs. This will provide feedback to optimization of the growth conditions and facilitate the large-scale production and high-quality monitoring in the future device fabrication process. However, adsorption or etching will more or less bring damage to the film samples.

2.3. High-Throughput Characterization by Optical Spectroscopy. Noninvasive, high-throughput spectroscopic techniques, including Raman, SHG, and PL, provide an efficient route for the characterization of large-area TMDs without transfer process and no special requirements for substrates.^{123–126} All these techniques can be classified into two main categories: (1) the defects can be detected by the differences of the characteristic peak in Raman and PL; (2) the defects in TMDs can be easily monitored by nonlinear optical processes such as SHG, which is very sensitive to non-centrosymmetric materials.

2.3.1. Raman Spectroscopy. Raman spectroscopy is a universal method to determine vibration modes and provide a structural fingerprint of molecules. Therefore, Raman spectroscopy is widely used to characterize the unique properties of 2D layered materials, such as the number of layers, the effect of external electric perturbation or doping, and thermal conductivities.^{127–129} Basically, monolayer 2H- MX_2 has three Raman active modes associated with the A_1' (A_{1g}), E' (E_{2g}^1) and E'' irreducible representations of the D_{3h} group. For the A_1' mode, the X atoms vibrate in the out-of-plane direction and the M atoms remain static. In addition, for the E' and E'' modes, the movements of all atoms are in plane. However, for the E' mode, the X atoms and M atoms move in opposite directions, while the E'' mode is related to the nonnull elements of the Raman tensor and does not appear in the commonly used Raman backscattering configuration. Therefore, the E_{2g}^1 and A_{1g} peaks are prominent Raman characteristic signals in the Raman spectra of monolayer TMDs. The typical phonon spectrum of MoS_2 is shown in Figure 4a.¹³⁰ The defects in the lattice structure will alter the phonon modes,

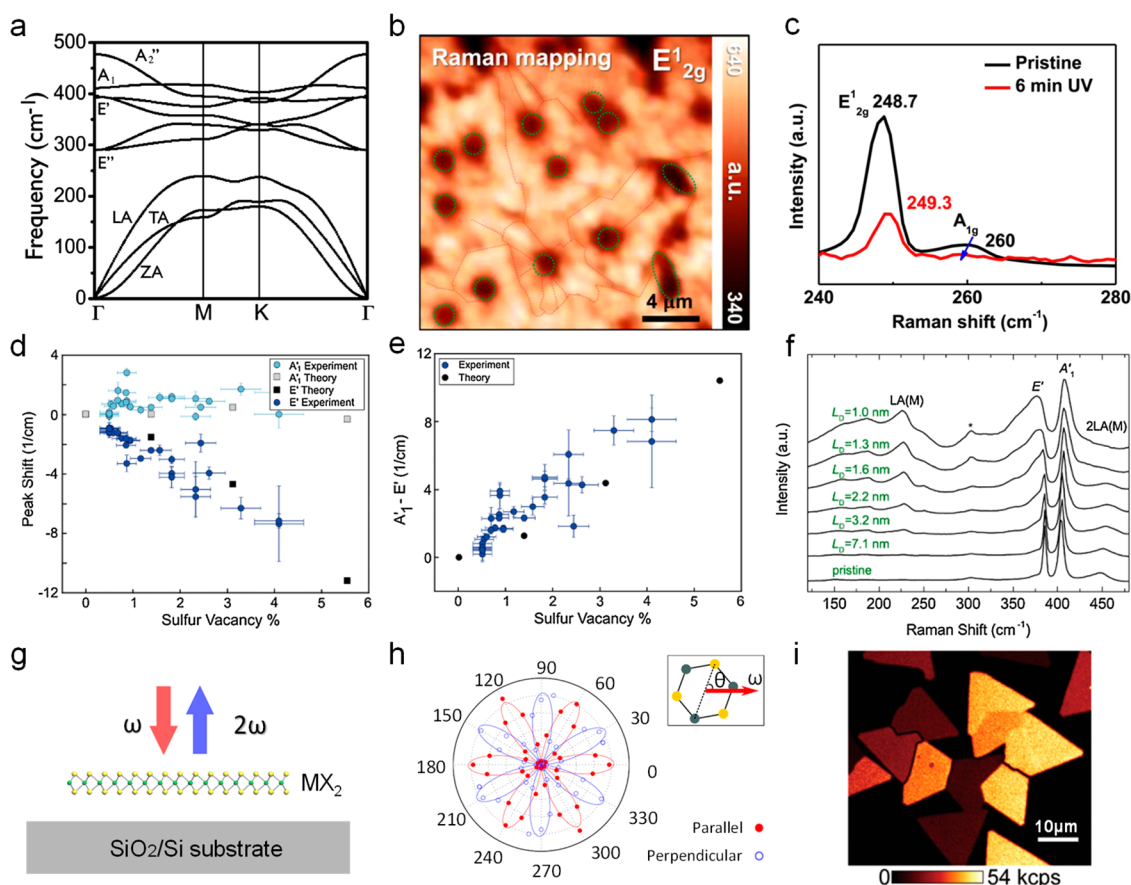


Figure 4. Raman spectroscopy and SHG in determining defects. (a) Phonon spectra of MoS₂. Reproduced with permission from ref 130. Copyright 2015 American Chemical Society. (b) Confocal Raman of WSe₂ exposed to UV treatment. (c) Raman peaks of pristine WSe₂ and WSe₂ exposed to UV light for 6 min. Parts b and c were reproduced with permission from ref 115. Copyright 2014 American Chemical Society. (d, e) Experimental and theoretical peak shifts of A' and E' versus sulfur vacancies in MoS₂. Reproduced with permission from ref 131. Copyright 2016 American Chemical Society. (f) Raman spectra of Mn⁺ bombarded MoS₂ with different defect densities. New peaks appear when increasing the defect density in MoS₂. Reproduced with permission from ref 128. Copyright 2015 American Physical Society. (g) Schematic diagram of the SHG process in MX₂ on a SiO₂/Si substrate. Reproduced with permission from ref 140. Copyright 2021 The Author(s), under exclusive license to Springer Nature Limited. (h) Polar plot of angular dependence SHG intensity from monolayer MoS₂. The red and blue patterns respectively show parallel and perpendicular components of the SHG signal, respectively. Reproduced with permission from ref 132. Copyright 2013 American Chemical Society. (i) SHG image of CVD-grown polycrystalline monolayer MoS₂. Reproduced with permission from ref 136. Copyright 2015 WILEY-VCH Verlag GmbH & Co. KGaA, Weinheim, Germany.

leading to the change of the Raman peak position. Moreover, the oscillating strength of the phonons can also be affected by the defect density, which leads to the intensity changes of Raman peaks.

Hence, Raman spectroscopy can be applied to monitor GBs in TMDs. For monolayer WSe₂ exposed to UV light with a humidity level of ~65% for 6 min, darker positions in the Raman mapping image related to GB regions are visible (Figure 4b).¹¹⁵ Correspondingly, the intensity of the E_{2g}¹ peak is weaker than that of pristine materials, and the location of this peak also shifts slightly. Furthermore, the intensity of the A_{1g} peak is also reduced (Figure 4c). In brief, this technique is a convenient and practical way to evaluate the effect of GBs in monolayer TMDs.

In addition, Raman spectroscopy can be used to detect point defects such as vacancies in TMDs. It has been reported that changes in the Raman modes vary with the number of S vacancies induced by electron beam irradiation in MoS₂.¹³¹ In-depth experimental characterizations and theoretical calculations show that the shift of E_{2g}¹ and A_{1g} is approximate linear correlation to sulfur vacancy concentration (Figure 4d,e). The

shift of the E_{2g}¹ peak is clearly more remarkable than the shift of the A_{1g} peak, indicating that the shift of the E_{2g}¹ peak is a better way to determine the S vacancy concentration. In addition, as shown in Figure 4e, the separation between these two peaks is an effective way to indicate the concentration of S vacancies. Furthermore, the appearance of new Raman peaks is a practical route to detect point defects of TMDs. The defect-induced new Raman scattering peaks arising in monolayer MoS₂ flakes by Mn⁺ ion bombardment have also been investigated.¹²⁸ As shown in Figure 4f, some new peaks appear when the density of defects increases. The most remarkable new peak is located at approximately 227 cm⁻¹, and the intensity is proportional to the density of defects.

2.3.2. Second Harmonic Generation. Nonlinear optical processes, especially SHG, are also a convenient way to detect defects in TMDs. SHG is the most fundamental process in nonlinear optics, which generates radiation at twice the frequency of the incident light. The SHG signal originates from different polarizations including electric dipoles, electric quadrupoles, and magnetic dipoles. These polarizations are dominated by the symmetry properties of crystalline materials.

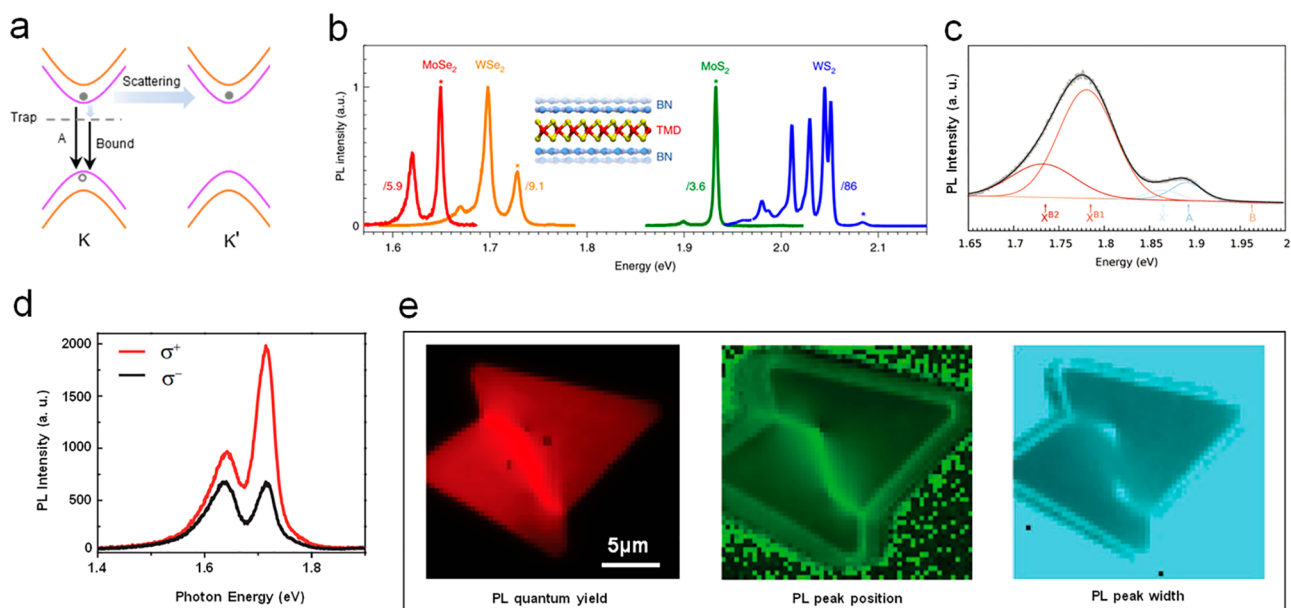


Figure 5. PL spectroscopy in determining defects. (a) Band structure of monolayer TMDs near the band gap. (b) PL spectra of high-quality mechanically exfoliated TMDs at a temperature of 7 K. The PL spectra feature multiple peaks, including emission from the A exciton, trion and defect trapped exciton. Reproduced with permission from ref 142. Copyright 2020 The Author(s), under exclusive license to Springer Nature Limited. (c) PL spectra of CVD grown WS_2 at a temperature of 7 K. The decrease in quality brings a broadened emission peak. Reproduced with permission from ref 143. Copyright 2020 The Royal Society of Chemistry. (d) Valley polarization of WSe_2 monolayer. Reproduced with permission from ref 148. Copyright 2017 American Physical Society. (e) PL characterization of a CVD grown MoS_2 sample. Reproduced with permission from ref 91. Copyright 2013 Nature Publishing Group.

The TMD monolayers have relatively large nonlinear susceptibility and noninversion symmetry. Therefore, the SHG signal has the capacity to acquire abundant information about the structural properties, especially the GBs and domain edges of TMDs.^{132–139}

A schematic diagram of the SHG experimental setup is shown in Figure 4g.¹⁴⁰ The MX_2 monolayer is excited by the input beam with frequency ω and generates an output beam with a frequency of 2ω . Monolayer MX_2 belongs to the D_{3h} point group with in-plane 3-fold rotation symmetry. The parallel and perpendicular components of the SHG signal are represented as $I_{\parallel} = I \cos^2(3\theta)$ and $I_{\perp} = I \sin^2(3\theta)$, respectively, where θ is the angle between the polarization direction and crystalline armchair direction. The maximum value of I_{\parallel} appears when the polarization of the excitation laser is parallel to the crystalline armchair direction (Figure 4h). Therefore, SHG exhibits considerable potential in GB visualization because of its sensitivity to symmetry variations. Figure 4i shows an SHG image of monolayer MoS_2 grown by the CVD method. The SHG intensity is reduced along the GBs as a result of destructive interference of waves from neighboring grains, thus, the GBs in SHG mapping are clearly visible.

2.3.3. Photoluminescence Spectroscopy. Monolayer TMDs can emit strong PL due to their direct bandgap nature and excitonic effects.¹⁴¹ The typical band structure of TMDs is sketched in Figure 5a. After monolayer TMDs are excited by a high-energy photon, carriers will rapidly relax to the substable excited state with the lowest energy, i.e., in an exciton state. An exciton is formed by an electron in the conduction band minimum and a hole in the valence band maximum located at the same valley with the opposite spin via attractive Coulomb interaction. Owing to the distinct states induced by various defects such as chalcogen vacancies, bound excitons induced by defects can also exist with lower energy. As for the

electronic states, the emergence of defects brings defect states between the conduction and valence bands and gives rise to the peak position deviation of PL. Besides, the increased nonradiative recombination rate caused by the defect states also leads to the PL intensity attenuation.

Typical PL spectra of high-quality mechanically exfoliated TMDs are shown in Figure 5b, where BN-encapsulation is used to reduce the impact on PL spectra from the substrate, and the experiment is performed at cryogenic temperatures below 20 K to reduce the broadening of spectra caused by phonons.¹⁴² The exciton peak labeled with “*” can be clearly separated from the defect state luminescence for every TMD material. By inserting a graphene layer, the defect peak can be filtered out. However, it is not possible to encapsulate every sample with BN, and the quality of the TMDs prepared in other ways is hard to compare with that of mechanically exfoliated TMDs.

For the CVD-grown TMD monolayer, the PL spectra will broaden (Figure 5c). It is expected that the intensity of the separated peaks can be used to evaluate the quality of the sample. A cryogenic broad PL spectrum is observed in CVD-grown MoS_2 which can be analyzed via multiple peak fitting. The whole spectrum can be divided into five peaks.¹⁴³ The bound exciton peaks $X^{\text{B}2}$ and $X^{\text{B}1}$ reflect the density of S vacancy defects.¹⁴⁴ The charged exciton peak X^- originates from the doping of the sample, where a negative charged exciton means a three-particle state consisting of two electrons and one hole.¹⁴⁵

The exciton peak A in the PL spectra is described above and shown in Figure 5b. The exciton peak B represents an exciton formed by an electron and a hole with spin opposite to those in the A exciton. Peak B has lower intensity than peak A and appears at a higher energy. After attaining the cryogenic PL spectrum of the sample, the intensity of the bound exciton

Table 1. Electrical Performances of Monolayer TMD-Based FETs at Room Temperature

method	TMDs	orientation	on/off ratio	field-effect mobility ($\text{cm}^2\text{V}^{-1}\text{s}^{-1}$)	SS (mV/dec)	ref
exfoliated	MoS ₂	single crystal	$>10^6$	44	410	170
exfoliated	WSe ₂	single crystal	$>10^6$	250	60	38
exfoliated	WS ₂	single crystal	–	83	–	171
exfoliated	MoSe ₂	single crystal	$>10^6$	50	–	172
MOCVD	MoS ₂	polycrystalline	10^7	46	76	173
MOCVD	WS ₂	polycrystalline	10^7	33	80	173
CVD	MoS ₂	highly oriented	10^9	70	–	162
CVD	MoS ₂	single crystal	10^9	102.6	210	163

peaks can be used to evaluate the density of S vacancies, which can be passivated easily by oxygen in air. The relative intensity of the A/B exciton peak ratio is also a useful index for defect density, because the lifetime of nonradiative recombination is shorter than that of radiative recombination for the A exciton and thus will significantly affect the intensity of the A exciton peak while only slightly affecting the B exciton peak because the latter has the shortest lifetime.¹⁴⁶

Simultaneously, valley polarization is one of the most famous unique optical properties of TMDs in 2H phase. As shown in Figure 5a, TMDs have two valleys with opposite optical circular polarization selectivity. If we excite the material with fully polarized photons, in most luminescence cases, the excitons will recombine in the same excitation valley. However, Coulomb interaction and some defect states, which can introduce intervalley scattering of excitons, make the PL spectrum not fully polarized.¹⁴⁷ A typical valley polarization spectrum of monolayer WSe₂ is shown in Figure 5d.¹⁴⁸ If defects affect the nonradiative recombination channel more than the intervalley scattering process, valley polarization degree will increase. However, some defect states can introduce intervalley scattering of excitons, and thus the degree of circular polarization may contrarily decrease.^{149,150} The valley polarization somewhat reflects the quality of the sample.

In addition to point defects such as the chalcogen vacancy mentioned above, GBs can be recognized by PL spectrum mapping.⁹¹ As shown in Figure 5e, the islands at the GBs show strong PL modifications including quantum yield, peak position, and PL peak width, which demonstrate that PL is strongly affected by the presence of GBs.

However, optical spectroscopy indeed has its own disadvantages. The spatial resolution of far field optical spectroscopy is limited by the laser spot size of ~ 500 nm. Besides, optical spectroscopy can also be influenced by other factors including strain, electron doping and substrate. In a word, Raman, SHG and PL are all fast and contactless techniques to uncover the quality-property relationships of 2D TMDs materials through characteristic peak or mapping. Among them, Raman spectra is the most sensitive technique to characterize point defects or GBs in the most TMDs that have Raman-active modes. PL spectra is widely used for characterizing defects in semiconducting materials through variations of the characteristic peak intensity and width. However, this method will be invalid for metallic materials and semiconductor with no luminescence. SHG is very powerful for identifying the crystal orientation, while this method can only be applied to central symmetry broken materials.

2.4. Electrical Transport Measurement by FETs.

Excellent electrical properties are a prerequisite for TMDs applied to electronic and optoelectronic devices in which the

FETs are the most fundamental elements.^{151–156} Thus, to characterize the electronic quality, TMDs-based FETs should be fabricated and tested accurately and scientifically. For a typical FET, the most important parameters are carrier mobility (μ), subthreshold swing (SS), and the on/off ratio ($I_{\text{on}}/I_{\text{off}}$). These three values are usually used to evaluate the electrical properties of TMDs. In principle, these three parameters are used to compare the electrical properties of the same TMD obtained by different methods. Generally, these three parameters are close to the theoretical value, which means that the TMD has relatively high quality. Therefore, greater carrier mobility, lower subthreshold swing, and higher on–off ratio mean better quality of measured samples of TMD, which result from less carriers scattering during transport in the crystal with fewer defects.

Although the electrical properties and electronic structure of TMDs have been studied since 1960s,¹⁵⁷ the application of related devices has been consistently limited. WSe₂ crystal was first applied to FETs until 2004.¹⁵⁸ The charge carrier mobility is up to $500 \text{ cm}^2 \text{ V}^{-1} \text{ S}^{-1}$ for the p-type conductivity in the WSe₂-based FETs at room temperature, comparable to that in the best single-crystal Si-based FETs. The first micro-mechanical exfoliated single-layer MoS₂-based FETs were fabricated in 2011.³⁷ The mobility of single-layer MoS₂ FETs with a hafnium oxide gate dielectric is at least $200 \text{ cm}^2 \text{ V}^{-1} \text{ S}^{-1}$.

In principle, the device performance of atomically thin TMD-based FETs depends on a variety of factors, such as the material quality, thickness, substrate, contacts, environment. Here we focus primarily on the effects of the material quality on the electrical transport characteristics. The electrical performances of monolayer TMD-based FETs at room temperature are summarized in Table 1. It is obvious that single crystal TMDs show excellent electrical properties. However, the mechanically exfoliated single crystal TMD devices are limited at a small scale, making them unfavorable for industrial applications.

With the development of growth methods, especially CVD, wafer-scale TMD monolayers provide a promising way to further implement realistic systems. For the first time, batch-fabricated MoS₂ FET devices on 4-in. MoS₂ films have been achieved and demonstrated the electrical uniformity of wafer-scale monolayer MoS₂ films grown by the metal–organic CVD (MOCVD) method.¹⁵⁹ All the devices show similar field-effect mobilities near $30 \text{ cm}^2 \text{ V}^{-1} \text{ s}^{-1}$ and a high on/off conductance ratio of approximately 10^6 . This makes it possible to realize atomically thin integrated circuitry. However, the tilt GBs in TMDs films reduce the electrical transport properties,^{91,160} resulting from the changes of electronic structure around the GBs.^{151,161}

Typical fabricated FET devices based on large-area MoS₂ show higher electrical quality at room temperature when MoS₂

has single-crystalline orientations. Highly oriented 4-in. monolayer MoS₂ FET devices have an average mobility of approximately 70 cm² V⁻¹ s⁻¹ and an on/off ratio of 10⁹ after transferred onto SiO₂.¹⁶² A 2-in. wafer-scale single-crystal MoS₂ grown on sapphire also shows higher performance in FETs.¹⁶³ The carrier mobility (102.6 cm² V⁻¹ s⁻¹) and saturation current (450 μA μm⁻¹) are the highest records among wafer-scale monolayer MoS₂ films by now. The FETs also show excellent uniformity in carrier mobility and subthreshold swing, with variations of 15 and 11%, respectively. The devices with a 500 nm channel length exhibited an SS of 210 mV dec⁻¹ and the I_{on}/I_{off} is nearly 10⁹. The statistical analysis of the mobility and SS also exhibits Gaussian distributions.

Moreover, it is a common strategy to improve the electronic properties of 2D semiconductors by repairing atomic defects and restoring the intrinsic lattice structure. A facile low-temperature thiol chemistry route is used to repair the sulfur vacancies in exfoliated MoS₂.¹⁶⁴ And, the mobility is up to 80 cm² V⁻¹ s⁻¹ in backgated monolayer MoS₂ FETs at room temperature. Meanwhile, it shows that the appropriate density of anion vacancies in TMDs could be beneficial to electronic properties.^{165–168} The latest study suggests that a record-high carrier mobility of ~115 cm² V⁻¹ s⁻¹ is achieved by systematically tailoring the sulfur vacancies to the appropriate density of 4.7% in the CVD-grown monolayer MoS₂.¹⁶⁹ Transistors based on this tailored MoS₂ exhibit an outstanding current density of >0.61 mA μm⁻¹ and a high on/off ratio of >10¹⁰. Ultimately, transistors need to be reliably manufactured in massive production, and the CVD method might be the most promising way to grow high uniformity and quality single crystal thin films.

In brief, 2D TMDs with abundant electronic band structure hold great promise for future electronic and optoelectronic devices. These applications are strongly dependent on the electrical properties of 2D materials-based FETs. High performance of these FETs means the quality of used materials is high. However, the assessment of ultrathin 2D layered materials based-FET performance remains challenges since some factors such as contact resistance, Schottky barrier, and metal doping will also bring unreliable results.

3. SUMMARY AND OUTLOOK

In this Review, we have highlighted four commonly used characterization techniques for monitoring the material quality of TMDs from nanoscale atomic structures to large-area visualization. In summary, each method has its advantages and drawbacks. TEM, STEM and AFM can provide accurate information of the defect structure with atomic-level spatial resolution, while they are time-consuming for a large-scale characterization. Selective etching and adsorption take the advantage of facile and large-scale fast imaging of defects, while they will more or less bring damage to the sample. Spectroscopic-based methods are fast, contactless, and non-destructive techniques, while they are limited by the spatial resolution and cannot directly give a correspondence between spectrum and defect types. FET can directly tell us the material quality from the view of devices, while the device parameters can also be significantly affected by the fabrication process. Therefore, the combination of different methods will be very comprehensive for the monitoring of material quality. Nonetheless, there is still a significant need to develop advanced techniques for defect engineering. For example, in

situ evaluation of defects during CVD grown or device operation for TMDs are highly needed but still currently lacking. Additionally, once the vacancy introduced during sample synthesis has been detected through characterization, how to repair them is the next question to be solved. Finally, a unified standard for a quality evaluation is waiting to be established for further industrialization.

AUTHOR INFORMATION

Corresponding Authors

Kaihui Liu – State Key Laboratory for Mesoscopic Physics, Frontiers Science Centre for Nano-optoelectronics, School of Physics, Peking University, Beijing 100871, China; Songshan Lake Materials Laboratory, Institute of Physics, Chinese Academy of Sciences, Dongguan 523808, China; orcid.org/0000-0002-8781-2495; Email: khliu@pku.edu.cn

Yun Zhao – School of Chemistry and Chemical Engineering, Beijing Institute of Technology, Beijing 102488, China; orcid.org/0000-0002-4432-9305; Email: zhaoyun@bit.edu.cn

Lena Du – Shenzhen Institute for Quantum Science and Engineering, and Department of Physics, Southern University of Science and Technology, Shenzhen 518055, China; Department of Physics, Capital Normal University, Beijing 100037, China; Email: duln@cnu.edu.cn

Authors

Jinhuan Wang – School of Chemistry and Chemical Engineering, Beijing Institute of Technology, Beijing 102488, China; orcid.org/0000-0001-5569-8520

Chen Huang – State Key Laboratory for Mesoscopic Physics, Frontiers Science Centre for Nano-optoelectronics, School of Physics, Peking University, Beijing 100871, China

Yilong You – State Key Laboratory for Mesoscopic Physics, Frontiers Science Centre for Nano-optoelectronics, School of Physics, Peking University, Beijing 100871, China

Quanlin Guo – State Key Laboratory for Mesoscopic Physics, Frontiers Science Centre for Nano-optoelectronics, School of Physics, Peking University, Beijing 100871, China

Guodong Xue – State Key Laboratory for Mesoscopic Physics, Frontiers Science Centre for Nano-optoelectronics, School of Physics, Peking University, Beijing 100871, China

Hao Hong – State Key Laboratory for Mesoscopic Physics, Frontiers Science Centre for Nano-optoelectronics, School of Physics, Peking University, Beijing 100871, China

Qingze Jiao – School of Chemistry and Chemical Engineering, Beijing Institute of Technology, Beijing 102488, China

Dapeng Yu – Shenzhen Institute for Quantum Science and Engineering, and Department of Physics, Southern University of Science and Technology, Shenzhen 518055, China

Complete contact information is available at: <https://pubs.acs.org/10.1021/acs.jpcc.2c00051>

Notes

The authors declare no competing financial interest.

Biographies

Jinhuan Wang is currently a Ph.D. candidate at the School of Chemistry and Chemical Engineering, Beijing Institute of Technology. Her research interests are focused on study of TMDs preparation and characterization.

Chen Huang is currently a Ph.D. student at the School of Physics, Peking University, China. His research focuses on the ultrafast carrier dynamics and nonlinear optics of low-dimensional materials.

Yilong You is currently a Ph.D. student at the School of Physics, Peking University, China. His research focuses on the ultrafast and nonlinear optics of low-dimensional materials.

Quanlin Guo is currently a Ph.D. student at the School of Physics, Peking University, China. Her research interests are focused on study of atomic and electronic structures of two-dimensional material by electron microscopy.

Guodong Xue is currently a Ph.D. student at the School of Physics, Peking University, China. His research focuses on the preparation and characterization of TMDs.

Hao Hong is currently a postdoctoral researcher in the State Key Lab for Mesoscopic Physics, School of Physics, Peking University, China. His research focuses on the ultrafast and nonlinear optics of low-dimensional materials.

Qingze Jiao is currently a professor in the School of Chemistry and Chemical Engineering, Beijing Institute of Technology. He received his Ph.D. from Jilin University in 1998. His current research interests are industrial catalysis, inorganic functionals, and new catalytic materials.

Dapeng Yu is an Academician of Chinese Academy of Sciences. He obtained his Ph.D. at the Laboratoire de Physique des Solides, Université de Paris-Sud, Orsay, France, 1992. He is currently a chair professor of the Physics Department, Southern University of Science and Technology and the dean of the Shenzhen Institute for Quantum Science and Engineering, China. His current research focuses on controllable preparation and quantum transport property measurement of quantum materials.

Lena Du is currently a lecturer in the Department of Physics, Capital Normal University, China. She received her Ph.D. from the National Center for Nanoscience and Technology, Chinese Academy of Sciences in 2019, and afterward worked as a postdoctoral research fellow at the Shenzhen Institute for Quantum Science and Engineering, China until 2021. Her current research is low dimensional material devices and physics.

Yun Zhao is currently a professor in the School of Chemistry and Chemical Engineering, Beijing Institute of Technology. She received her Ph.D. from the Beijing University of Chemical Technology in 2002. Her current research interests are the design, synthesis, and application of polymer materials.

Kaihui Liu is currently a professor and principle investigator in the State Key Lab for Mesoscopic Physics, School of Physics, Peking University, China. He received his Ph.D. from the Institute of Physics, Chinese Academy of Sciences in 2009 and afterward worked as a postdoctoral research fellow at UC Berkeley, United States, until 2014. His current research interests are the growth, characterization, and applications of meter-scale single crystals.

ACKNOWLEDGMENTS

This work was supported by the Key R&D Program of Guangdong Province (2019B010931001, 2020B010189001, and 2018B030327001), the National Natural Science Foundation of China (92163206, 52025023, 51991342, 52021006, 51991344, 52100115, and 11888101), the China Postdoctoral Science Foundation (2021T140022), the Strategic Priority Research Program of the Chinese Academy of Sciences (XDB33000000), the Beijing Natural Science

Foundation (JQ19004), and the Pearl River Talent Recruitment Program of Guangdong Province (2019ZT08C321).

REFERENCES

- (1) Mattheiss, L. F. Band structures of transition-metal-dichalcogenide layer compounds. *Phys. Rev. B* **1973**, *8*, 3719–3740.
- (2) Frindt, R. T.; Yoffe, A. D. Physical properties of layer structures: optical properties and photoconductivity of thin crystals of molybdenum disulphide. *Proc. R. Soc. A* **1963**, *273*, 69–83.
- (3) Joensen, P.; Frindt, R. F.; Morrison, S. R. Single-layer MoS₂. *Mater. Res. Bull.* **1986**, *21*, 457–461.
- (4) Novoselov, K. S.; Geim, A. K.; Morozov, S. V.; Jiang, D.; Zhang, Y.; Dubonos, S. V.; Grigorieva, V.; Firsov, A. A. Electric field effect in atomically thin carbon films. *Science* **2004**, *306*, 666–669.
- (5) Li, T.; Galli, G. Electronic properties of MoS₂ nanoparticles. *J. Phys. Chem. C* **2007**, *111*, 16192–16196.
- (6) Mak, K. F.; Lee, C.; Hone, J.; Shan, J.; Heinz, T. F. Atomically thin MoS₂: a new direct-gap semiconductor. *Phys. Rev. Lett.* **2010**, *105*, 136805.
- (7) Splendiani, A.; Sun, L.; Zhang, Y. B.; Li, T.; Kim, J.; Chim, C. Y.; Galli, G.; Wang, F. Emerging photoluminescence in monolayer MoS₂. *Nano Lett.* **2010**, *10*, 1271–1275.
- (8) Wang, Q. H.; Kalantar-Zadeh, K.; Kis, A.; Coleman, J. N.; Strano, M. S. Electronics and optoelectronics of two-dimensional transition metal dichalcogenides. *Nat. Nanotechnol.* **2012**, *7*, 699–712.
- (9) Cheiwchanmangij, T.; Lambrecht, W. R. L. Quasiparticle band structure calculation of monolayer, bilayer, and bulk MoS₂. *Phys. Rev. B* **2012**, *85*, 205302.
- (10) Kuc, A. Low-dimensional transition-metal dichalcogenides. *Chem. Modell.* **2014**, *11*, 1–29.
- (11) Kuc, A.; Heine, T.; Kis, A. Electronic properties of transition-metal dichalcogenides. *MRS Bull.* **2015**, *40*, 577–584.
- (12) Lee, J.; Mak, K. F.; Shan, J. Electrical control of the valley Hall effect in bilayer MoS₂ transistors. *Nat. Nanotechnol.* **2016**, *11*, 421–425.
- (13) Chhowalla, M.; Jena, D.; Zhang, H. Two-dimensional semiconductors for transistors. *Nat. Rev. Mater.* **2016**, *1*, 16052.
- (14) Cao, T.; Wang, G.; Han, W. P.; Ye, H. Q.; Zhu, C. R.; Shi, J.; Niu, Q.; Tan, P. H.; Wang, E.; Liu, B. L.; et al. Valley-selective circular dichroism of monolayer molybdenum disulphide. *Nat. Commun.* **2012**, *3*, 887.
- (15) Zeng, H. L.; Dai, J. F.; Yao, W.; Xiao, D.; Cui, X. D. Valley polarization in MoS₂ monolayers by optical pumping. *Nat. Nanotechnol.* **2012**, *7*, 490–493.
- (16) Xiao, D.; Liu, G. B.; Feng, W. X.; Xu, X. D.; Yao, W. Coupled spin and valley physics in monolayers of MoS₂ and other group-VI dichalcogenides. *Phys. Rev. Lett.* **2012**, *108*, 196802.
- (17) Mak, K. F.; He, K. L.; Shan, J.; Heinz, T. F. Control of valley polarization in monolayer MoS₂ by optical helicity. *Nat. Nanotechnol.* **2012**, *7*, 494–498.
- (18) Schaibley, J. R.; Yu, H.; Clark, G.; Rivera, P.; Ross, J. S.; Seyler, K. L.; Yao, W.; Xu, X. Valleytronics in 2D materials. *Nat. Rev. Mater.* **2016**, *1*, 16055.
- (19) Liu, X. Z.; Galfsky, T.; Sun, Z.; Xia, F.; Lin, E. C.; Lee, Y.-H.; Kéna-Cohen, S.; Menon, V. M. Strong light–matter coupling in two-dimensional atomic crystals. *Nat. Photonics* **2015**, *9*, 30–34.
- (20) Schwarz, S.; Dufferwiel, S.; Walker, P. M.; Withers, F.; Trichet, A. A.; Sich, M.; Li, F.; Chekhovich, E. A.; Borisenko, D. N.; Kolesnikov, N. N.; et al. Two-dimensional metal-chalcogenide films in tunable optical microcavities. *Nano Lett.* **2014**, *14*, 7003–7008.
- (21) Wu, S.; Buckley, S.; Schaibley, J. R.; Feng, L.; Yan, J.; Mandrus, D. G.; Hatami, F.; Yao, W.; Vuckovic, J.; Majumdar, A.; et al. Monolayer semiconductor nanocavity lasers with ultralow thresholds. *Nature* **2015**, *520*, 69–72.
- (22) Ye, Y.; Wong, Z. J.; Lu, X. F.; Ni, X.; Zhu, H.; Chen, X.; Wang, Y.; Zhang, X. Monolayer excitonic laser. *Nat. Photonics* **2015**, *9*, 733–737.

- (23) Salehzadeh, O.; Djavid, M.; Tran, N. H.; Shih, I.; Mi, Z. Optically pumped two-dimensional MoS₂ lasers operating at room-temperature. *Nano Lett.* **2015**, *15*, 5302–5306.
- (24) Hanlon, D.; Backes, C.; Higgins, T. M.; Hughes, M.; O'Neill, A.; King, P.; McEvoy, N.; Duesberg, G. S.; Mendoza Sanchez, B.; Pettersson, H.; et al. Production of molybdenum trioxide nanosheets by liquid exfoliation and their application in high-performance supercapacitors. *Chem. Mater.* **2014**, *26*, 1751–1763.
- (25) Tang, H. J.; Wang, J. Y.; Yin, H. J.; Zhao, H.; Wang, D.; Tang, Z. Growth of polypyrrole ultrathin films on MoS₂ monolayers as high-performance supercapacitor electrodes. *Adv. Mater.* **2015**, *27*, 1117–1123.
- (26) Acerce, M.; Voiry, D.; Chhowalla, M. Metallic 1T phase MoS₂ nanosheets as supercapacitor electrode materials. *Nat. Nanotechnol.* **2015**, *10*, 313–318.
- (27) Zhang, B.; Ji, X.; Xu, K.; Chen, C.; Xiong, X.; Xiong, J.; Yao, Y.; Miao, L.; Jiang, J. Unraveling the different charge storage mechanism in T and H phases of MoS₂. *Electrochim. Acta* **2016**, *217*, 1–8.
- (28) Bissett, M. A.; Worrall, S. D.; Kinloch, I. A.; Dryfe, R. A. W. Comparison of two-dimensional transition metal dichalcogenides for electrochemical supercapacitors. *Electrochim. Acta* **2016**, *201*, 30–37.
- (29) Wang, Y.; Yu, L.; Lou, X. W. Synthesis of highly uniform molybdenum-glycerate spheres and their conversion into hierarchical MoS₂ hollow nanospheres for lithium-ion batteries. *Angew. Chem., Int. Ed.* **2016**, *55*, 7423–7426.
- (30) Lopez-Sanchez, O.; Lembke, D.; Kayci, M.; Radenovic, A.; Kis, A. Ultrasensitive photodetectors based on monolayer MoS₂. *Nat. Nanotechnol.* **2013**, *8*, 497–501.
- (31) Zhang, Y. J.; Oka, T.; Suzuki, R.; Ye, J. T.; Iwasa, Y. Electrically switchable chiral light-emitting transistor. *Science* **2014**, *344*, 725–728.
- (32) Withers, F.; Del Pozo-Zamudio, O.; Schwarz, S.; Dufferwiel, S.; Walker, P. M.; Godde, T.; Rooney, A. P.; Gholinia, A.; Woods, C. R.; Blake, P.; et al. WSe₂ light-emitting tunneling transistors with enhanced brightness at room temperature. *Nano Lett.* **2015**, *15*, 8223–8228.
- (33) Wang, H. N.; Zhang, C. J.; Chan, W. M.; Tiwari, S.; Rana, F. Ultrafast response of monolayer molybdenum disulfide photodetectors. *Nat. Commun.* **2015**, *6*, 8831.
- (34) Nalwa, H. S. A review of molybdenum disulfide (MoS₂) based photodetectors: from ultra-broadband, self-powered to flexible devices. *RSC Adv.* **2020**, *10*, 30529–30602.
- (35) Li, C.; Zhu, J.; Du, W.; Huang, Y.; Xu, H.; Zhai, Z.; Zou, G. The photodetectors based on lateral monolayer MoS₂/WS₂ heterojunctions. *Nanoscale Res. Lett.* **2021**, *16*, 123.
- (36) Taffelli, A.; Dire, S.; Quaranta, A.; Pancheri, L. MoS₂ based photodetectors: a review. *Sensors* **2021**, *21*, 2758.
- (37) Radisavljevic, B.; Radenovic, A.; Brivio, J.; Giacometti, V.; Kis, A. Single-layer MoS₂ transistors. *Nat. Nanotechnol.* **2011**, *6*, 147–150.
- (38) Fang, H.; Chuang, S.; Chang, T. C.; Takei, K.; Takahashi, T.; Javey, A. High-performance single layered WSe₂ p-FETs with chemically doped contacts. *Nano Lett.* **2012**, *12*, 3788–3792.
- (39) Kim, S.; Konar, A.; Hwang, W. S.; Lee, J. H.; Lee, J.; Yang, J.; Jung, C.; Kim, H.; Yoo, J. B.; Choi, J. Y.; et al. High-mobility and low-power thin-film transistors based on multilayer MoS₂ crystals. *Nat. Commun.* **2012**, *3*, 1011.
- (40) Ovchinnikov, D.; Allain, A.; Huang, Y.-S.; Dumcenco, D.; Kis, A. Electrical transport properties of single-layer WS₂. *ACS Nano* **2014**, *8*, 8174–8181.
- (41) Mir, S. H.; Yadav, V. K.; Singh, J. K. Recent advances in the carrier mobility of two-dimensional materials: a theoretical perspective. *ACS Omega* **2020**, *5*, 14203–14211.
- (42) Li, H.; Wu, J.; Yin, Z. Y.; Zhang, H. Preparation and applications of mechanically exfoliated single-layer and multilayer MoS₂ and WSe₂ nanosheets. *Acc. Chem. Res.* **2014**, *47*, 1067–1075.
- (43) Huang, Y.; Sutter, E.; Shi, N. N.; Zheng, J. B.; Yang, T. Z.; Englund, D.; Gao, H.-J.; Sutter, P. Reliable exfoliation of large-area high-quality flakes of graphene and other two-dimensional materials. *ACS Nano* **2015**, *9*, 10612–10620.
- (44) Magda, G. Z.; Peto, J.; Dobrik, G.; Hwang, C.; Biro, L. P.; Tapasztó, L. Exfoliation of large-area transition metal chalcogenide single layers. *Sci. Rep.* **2015**, *5*, 14714.
- (45) Desai, S. B.; Madhvapathy, S. R.; Amani, M.; Kiriya, D.; Hettick, M.; Tosun, M.; Zhou, Y.; Dubey, M., III; Ager, J. W.; Chrzan, D.; et al. Gold-mediated exfoliation of ultralarge optoelectronically-perfect monolayers. *Adv. Mater.* **2016**, *28*, 4053–4058.
- (46) Velicky, M.; Donnelly, G. E.; Hendren, W. R.; McFarland, S.; Scullion, D.; DeBenedetti, W. J. I.; Correa, G. C.; Han, Y.; Wain, A. J.; Hines, M. A.; et al. Mechanism of gold-assisted exfoliation of centimeter-sized transition-metal dichalcogenide monolayers. *ACS Nano* **2018**, *12*, 10463–10472.
- (47) Liu, Y.; Guo, J.; Zhu, E.; Liao, L.; Lee, S. J.; Ding, M.; Shakir, I.; Gambin, V.; Huang, Y.; Duan, X. Approaching the Schottky-Mott limit in van der Waals metal-semiconductor junctions. *Nature* **2018**, *557*, 696–700.
- (48) Huang, Y.; Pan, Y. H.; Yang, R.; Bao, L. H.; Meng, L.; Luo, H. L.; Cai, Y. Q.; Liu, G. D.; Zhao, W. J.; Zhou, Z.; et al. Universal mechanical exfoliation of large-area 2D crystals. *Nat. Commun.* **2020**, *11*, 2453.
- (49) Liong, F.; Wu, W. J.; Bai, Y. S.; Chae, S. H.; Li, Q.; Wang, J.; Hone, J.; Zhu, X. Y. Disassembling 2D van der Waals crystals into macroscopic monolayers and reassembling into artificial lattices. *Science* **2020**, *367*, 903–906.
- (50) Gordon, R. A.; Yang, D.; Crozier, E. D.; Jiang, D. T.; Frindt, R. F. Structures of exfoliated single layers of WS₂, MoS₂, and MoSe₂ in aqueous suspension. *Phys. Rev. B* **2002**, *65*, 125407.
- (51) Coleman, J. N.; Lotya, M.; O'Neill, A.; Bergin, S. D.; King, P. J.; Khan, U.; Young, K.; Gaucher, A.; De, S.; Smith, R. J.; et al. Two-dimensional nanosheets produced by liquid exfoliation of layered materials. *Science* **2011**, *331*, 568–571.
- (52) Nicolosi, V.; Chhowalla, M.; Kanatzidis, M. G.; Strano, M. S.; Coleman, J. N. Liquid exfoliation of layered materials. *Science* **2013**, *340*, 1226419.
- (53) Koma, A.; Yoshimura, K. Ultrasharp interfaces grown with Van der Waals epitaxy. *Surf. Sci.* **1986**, *174*, 556–560.
- (54) Ohuchi, F. S.; Shimada, T.; Parkinson, B. A.; Ueno, K.; Koma, A. Growth of MoSe₂ thin-films with Van der Waals epitaxy. *J. Cryst. Growth* **1991**, *111*, 1033–1037.
- (55) Lehtinen, O.; Komsa, H.-P.; Pulkin, A.; Whitwick, M. B.; Chen, M. W.; Lehnert, T.; Mohn, M. J.; Zazyev, O. V.; Kis, A.; Kaiser, U.; et al. Atomic scale microstructure and properties of Se-deficient two-dimensional MoSe₂. *ACS Nano* **2015**, *9*, 3274–3283.
- (56) Roy, A.; Movva, H. C.; Satpati, B.; Kim, K.; Dey, R.; Rai, A.; Pramanik, T.; Guchhait, S.; Tutuc, E.; Banerjee, S. K. Structural and electrical properties of MoTe₂ and MoSe₂ grown by molecular beam epitaxy. *ACS Appl. Mater. Interfaces* **2016**, *8*, 7396–7402.
- (57) Fu, D.; Zhao, X.; Zhang, Y. Y.; Li, L.; Xu, H.; Jang, A. R.; Yoon, S. I.; Song, P.; Poh, S. M.; Ren, T.; et al. Molecular beam epitaxy of highly crystalline monolayer molybdenum disulfide on hexagonal boron nitride. *J. Am. Chem. Soc.* **2017**, *139*, 9392–9400.
- (58) Zhan, Y. J.; Liu, Z.; Najmaei, S.; Ajayan, P. M.; Lou, J. Large-area vapor-phase growth and characterization of MoS₂ atomic layers on a SiO₂ substrate. *Small* **2012**, *8*, 966–971.
- (59) Liu, K. K.; Zhang, W. J.; Lee, Y. H.; Lin, Y. C.; Chang, M. T.; Su, C. Y.; Chang, C. S.; Li, H.; Shi, Y.; Zhang, H.; et al. Growth of large-area and highly crystalline MoS₂ thin layers on insulating substrates. *Nano Lett.* **2012**, *12*, 1538–1544.
- (60) Tang, L.; Li, T.; Luo, Y. T.; Feng, S.; Cai, Z.; Zhang, H.; Liu, B.; Cheng, H. M. Vertical chemical vapor deposition growth of highly uniform 2D transition metal dichalcogenides. *ACS Nano* **2020**, *14*, 4646–4653.
- (61) Zhou, J. D.; Lin, J. H.; Huang, X. W.; Zhou, Y.; Chen, Y.; Xia, J.; Wang, H.; Xie, Y.; Yu, H.; Lei, J.; et al. A library of atomically thin metal chalcogenides. *Nature* **2018**, *556*, 355–359.
- (62) He, T. Y.; Li, Y. J.; Zhou, Z. F.; Zeng, C.; Qiao, L.; Lan, C. Y.; Yin, Y.; Li, C.; Liu, Y. Synthesis of large-area uniform MoS₂ films by substrate-moving atmospheric pressure chemical vapor deposition: from monolayer to multilayer. *2D Mater.* **2019**, *6*, No. 025030.

- (63) Wang, J. H.; Xu, X. Z.; Cheng, T.; Gu, L. H.; Qiao, R. X.; Liang, Z. H.; Ding, D. D.; Hong, H.; Zheng, P. M.; Zhang, Z. B.; et al. Dual-coupling-guided epitaxial growth of wafer-scale single-crystal WS₂ monolayer on vicinal a-plane sapphire. *Nat. Nanotechnol.* **2022**, *17*, 33–38.
- (64) Lin, Z.; Mc Creary, A.; Briggs, N.; Subramanian, S.; Zhang, K. H.; Sun, Y. F.; Li, X. F.; Borys, N. J.; Yuan, H. T.; Fullerton-Shirey, S. K.; et al. 2D materials advances: from large scale synthesis and controlled heterostructures to improved characterization techniques, defects and applications. *2D Mater.* **2016**, *3*, No. 042001.
- (65) Yang, S. H.; Choi, W.; Cho, B. W.; Agyapong-Fordjour, F. O.; Park, S.; Yun, S. J.; Kim, H. J.; Han, Y. K.; Lee, Y. H.; Kim, K. K.; et al. Deep learning-assisted quantification of atomic dopants and defects in 2D materials. *Adv. Sci.* **2021**, *8*, 2101099.
- (66) Barja, S.; Refaely-Abramson, S.; Schuler, B.; Qiu, D. Y.; Pulkin, A.; Wickenburg, S.; Ryu, H.; Ugeda, M. M.; Kastl, C.; Chen, C.; et al. Identifying substitutional oxygen as a prolific point defect in monolayer transition metal dichalcogenides. *Nat. Commun.* **2019**, *10*, 3382.
- (67) Rhoads, D.; Chae, S. H.; Ribeiro-Palau, R.; Hone, J. Disorder in van der Waals heterostructures of 2D materials. *Nat. Mater.* **2019**, *18*, 541–549.
- (68) Liang, Q.; Zhang, Q.; Zhao, X.; Liu, M.; Wee, A. T. S. Defect engineering of two-dimensional transition-metal dichalcogenides: applications, challenges, and opportunities. *ACS Nano* **2021**, *15*, 2165–2181.
- (69) He, Y.; Tang, P.; Hu, Z.; He, Q.; Zhu, C.; Wang, L.; Zeng, Q.; Golani, P.; Gao, G.; Fu, W.; et al. Engineering grain boundaries at the 2D limit for the hydrogen evolution reaction. *Nat. Commun.* **2020**, *11*, 57.
- (70) Yao, W.; Wu, B.; Liu, Y. Growth and grain boundaries in 2D materials. *ACS Nano* **2020**, *14*, 9320–9346.
- (71) Reifsnnyder Hickey, D.; Nayir, N.; Chubarov, M.; Choudhury, T. H.; Bachu, S.; Miao, L.; Wang, Y.; Qian, C.; Crespi, V. H.; Redwing, J. M.; et al. Illuminating invisible grain boundaries in coalesced single-orientation WS₂ monolayer films. *Nano Lett.* **2021**, *21*, 6487–6495.
- (72) Tongay, S.; Suh, J.; Ataca, C.; Fan, W.; Luce, A.; Kang, J. S.; Liu, J.; Ko, C.; Raghunathanan, R.; Zhou, J.; et al. Defects activated photoluminescence in two-dimensional semiconductors: interplay between bound, charged, and free excitons. *Sci. Rep.* **2013**, *3*, 2657.
- (73) Zhang, Z. H.; Zou, X. L.; Crespi, V. H.; Yakobson, B. I. Intrinsic magnetism of grain boundaries in two-dimensional metal dichalcogenides. *ACS Nano* **2013**, *7*, 10475–10481.
- (74) McDonnell, S.; Addou, R.; Buie, C.; Wallace, R. M.; Hinkle, C. L. Defect-dominated doping and contact resistance in MoS₂. *ACS Nano* **2014**, *8*, 2880–2888.
- (75) Dang, K. Q.; Spearot, D. E. Effect of point and grain boundary defects on the mechanical behavior of monolayer MoS₂ under tension via atomistic simulations. *J. Appl. Phys.* **2014**, *116*, 013508.
- (76) Huang, Y. L.; Chen, Y.; Zhang, W.; Quek, S. Y.; Chen, C. H.; Li, L. J.; Hsu, W. T.; Chang, W. H.; Zheng, Y. J.; Chen, W.; et al. Bandgap tunability at single-layer molybdenum disulfide grain boundaries. *Nat. Commun.* **2015**, *6*, 6298.
- (77) Sangwan, V. K.; Jariwala, D.; Kim, I. S.; Chen, K. S.; Marks, T. J.; Lauhon, L. J.; Hersam, M. C. Gate-tunable memristive phenomena mediated by grain boundaries in single-layer MoS₂. *Nat. Nanotechnol.* **2015**, *10*, 403–406.
- (78) Zou, X.; Yakobson, B. I. An open canvas—2D materials with defects, disorder, and functionality. *Acc. Chem. Res.* **2015**, *48*, 73–80.
- (79) Rong, Y. M.; Sheng, Y. W.; Pacios, M.; Wang, X. C.; He, Z. Y.; Bhaskaran, H.; Warner, J. H. Electroluminescence dynamics across grain boundary regions of monolayer tungsten disulfide. *ACS Nano* **2016**, *10*, 1093–1100.
- (80) Ghorbani-Asl, M.; Enyashin, A. N.; Kuc, A.; Seifert, G.; Heine, T. Defect-induced conductivity anisotropy in MoS₂ monolayers. *Phys. Rev. B* **2013**, *88*, 245440.
- (81) Amani, M.; Lien, D.-H.; Kiriya, D.; Xiao, J.; Azcatal, A.; Noh, J.; Madhupathy, S. R.; Addou, R.; KC, S.; Dubey, M.; et al. Near-unity photoluminescence quantum yield in MoS₂. *Science* **2015**, *350*, 1065–1068.
- (82) Koperski, M.; Nogajewski, K.; Arora, A.; Cherkez, V.; Mallet, P.; Veuillen, J. Y.; Marcus, J.; Kossacki, P.; Potemski, M. Single photon emitters in exfoliated WSe₂ structures. *Nat. Nanotechnol.* **2015**, *10*, 503–506.
- (83) Jaramillo, T. F.; Jørgensen, K. P.; Bonde, J.; Nielsen, J. H.; Horch, S.; Chorkendorff, I. Identification of active edge sites for electrochemical H₂ evolution from MoS₂ nanocatalysts. *Science* **2007**, *317*, 100–102.
- (84) Li, H.; Tsai, C.; Koh, A. L.; Cai, L. L.; Contryman, A. W.; Fragapane, A. H.; Zhao, J. H.; Han, H. S.; Manoharan, H. C.; Abild-Pedersen, F.; et al. Activating and optimizing MoS₂ basal planes for hydrogen evolution through the formation of strained sulphur vacancies. *Nat. Mater.* **2016**, *15*, 48–53.
- (85) Voiry, D.; Fullon, R.; Yang, J.; de Carvalho Castro e Silva, C.; Kappera, R.; Bozkurt, I.; Kaplan, D.; Lagos, M. J.; Batson, P. E.; Gupta, G.; et al. The role of electronic coupling between substrate and 2D MoS₂ nanosheets in electrocatalytic production of hydrogen. *Nat. Mater.* **2016**, *15*, 1003–1009.
- (86) Li, G. Q.; Zhang, D.; Qiao, Q.; Yu, Y. F.; Peterson, D.; Zafar, A.; Kumar, R.; Curtarolo, S.; Hunte, F.; Shannon, S.; et al. All the catalytic active sites of MoS₂ for hydrogen evolution. *J. Am. Chem. Soc.* **2016**, *138*, 16632–16638.
- (87) Wang, S.; Robertson, A.; Warner, J. H. Atomic structure of defects and dopants in 2D layered transition metal dichalcogenides. *Chem. Soc. Rev.* **2018**, *47*, 6764–6794.
- (88) Mendes, R. G.; Pang, J. B.; Bachmatiuk, A.; Ta, H. Q.; Zhao, L.; Gemming, T.; Fu, L.; Liu, Z. F.; Rummeli, M. H. Electron-driven in situ transmission electron microscopy of 2D transition metal dichalcogenides and their 2D heterostructures. *ACS Nano* **2019**, *13*, 978–995.
- (89) Komsa, H. P.; Kotakoski, J.; Kurasch, S.; Lehtinen, O.; Kaiser, U.; Krasheninnikov, A. V. Two-dimensional transition metal dichalcogenides under electron irradiation: defect production and doping. *Phys. Rev. Lett.* **2012**, *109*, No. 035503.
- (90) Qiu, H.; Xu, T.; Wang, Z. L.; Ren, W.; Nan, H.; Ni, Z.; Chen, Q.; Yuan, S.; Miao, F.; Song, F.; et al. Hopping transport through defect-induced localized states in molybdenum disulfide. *Nat. Commun.* **2013**, *4*, 2642.
- (91) van der Zande, A. M.; Huang, P. Y.; Chenet, D. A.; Berkelbach, T. C.; You, Y. M.; Lee, G. H.; Heinz, T. F.; Reichman, D. R.; Muller, D. A.; Hone, J. C. Grains and grain boundaries in highly crystalline monolayer molybdenum disulfide. *Nat. Mater.* **2013**, *12*, 554–561.
- (92) Zhao, X.; Ning, S.; Fu, W.; Pennycook, S. J.; Loh, K. P. Differentiating polymorphs in molybdenum disulfide via electron microscopy. *Adv. Mater.* **2018**, *30*, 1802397.
- (93) Zhu, D. C.; Shu, H. B.; Jiang, F.; Lv, D. H.; Asokan, V.; Omar, O.; Yuan, J.; Zhang, Z.; Jin, C. H. Capture the growth kinetics of CVD growth of two-dimensional MoS₂. *npj 2D Mater. Appl.* **2017**, *1*, 1–7.
- (94) Zhao, X.; Song, P.; Wang, C.; Riis-Jensen, A. C.; Fu, W.; Deng, Y.; Wan, D.; Kang, L.; Ning, S.; Dan, J.; et al. Engineering covalently bonded 2D layered materials by self-intercalation. *Nature* **2020**, *581*, 171–177.
- (95) Lopatin, S.; Aljarb, A.; Roddatis, V.; Meyer, T.; Wan, Y.; Fu, J.-H.; Hedhili, M.; Han, Y.; Li, L.-J.; Tung, V. Aberration-corrected STEM imaging of 2D materials: artifacts and practical applications of threefold astigmatism. *Sci. Adv.* **2020**, *6*, 1–9.
- (96) Zhou, W.; Zou, X.; Najmaei, S.; Liu, Z.; Shi, Y.; Kong, J.; Lou, J.; Ajayan, P. M.; Yakobson, B. I.; Idrobo, J. C. Intrinsic structural defects in monolayer molybdenum disulfide. *Nano Lett.* **2013**, *13*, 2615–2622.
- (97) Hong, J. H.; Hu, Z. X.; Probert, M.; Li, K.; Lv, D.; Yang, X.; Gu, L.; Mao, N.; Feng, Q.; Xie, L.; et al. Exploring atomic defects in molybdenum disulfide monolayers. *Nat. Commun.* **2015**, *6*, 6293.
- (98) Lim, Y. F.; Priyadarshi, K.; Bussolotti, F.; Gogoi, P. K.; Cui, X.; Yang, M.; Pan, J.; Tong, S. W.; Wang, S.; Pennycook, S. J.; et al. Modification of vapor phase concentrations in MoS₂ growth using a NiO foam barrier. *ACS Nano* **2018**, *12*, 1339–1349.

- (99) Edelberg, D.; Rhodes, D.; Kerelsky, A.; Kim, B.; Wang, J.; Zangiabadi, A.; Kim, C.; Abhinandan, A.; Ardelean, J.; Scully, M.; et al. Approaching the intrinsic limit in transition metal diselenides via point defect control. *Nano Lett.* **2019**, *19*, 4371–4379.
- (100) Shree, S.; George, A.; Lehnert, T.; Neumann, C.; Benelajla, M.; Robert, C.; Marie, X.; Watanabe, K.; Taniguchi, T.; Kaiser, U.; et al. High optical quality of MoS₂ monolayers grown by chemical vapor deposition. *2D Mater.* **2020**, *7*, No. 015011.
- (101) Komsa, H.-P.; Kurasch, S.; Lehtinen, O.; Kaiser, U.; Krasheninnikov, A. V. From point to extended defects in two-dimensional MoS₂: Evolution of atomic structure under electron irradiation. *Phys. Rev. B* **2013**, *88*, No. 035301.
- (102) Lin, J. H.; Pantelides, S. T.; Zhou, W. Vacancy-induced formation and growth of inversion domains in transition-metal dichalcogenide monolayer. *ACS Nano* **2015**, *9*, 5189–5197.
- (103) Wang, S. S.; Qin, Z.; Jung, G. S.; Martin-Martinez, F. J.; Zhang, K.; Buehler, M. J.; Warner, J. H. Atomically sharp crack tips in monolayer MoS₂ and their enhanced toughness by vacancy defects. *ACS Nano* **2016**, *10*, 9831–9839.
- (104) Wang, S. S.; Lee, G. D.; Lee, S.; Yoon, E.; Warner, J. H. Detailed atomic reconstruction of extended line defects in monolayer MoS₂. *ACS Nano* **2016**, *10*, 5419–5430.
- (105) Najmaei, S.; Liu, Z.; Zhou, W.; Zou, X.; Shi, G.; Lei, S.; Yakobson, B. I.; Idrobo, J. C.; Ajayan, P. M.; Lou, J. Vapour phase growth and grain boundary structure of molybdenum disulphide atomic layers. *Nat. Mater.* **2013**, *12*, 754–759.
- (106) Lin, Y.-C.; Björkman, T.; Komsa, H.-P.; Teng, P.-Y.; Yeh, C.-H.; Huang, F.-S.; Lin, K.-H.; Jadcak, J.; Huang, Y.-S.; Chiu, P.-W.; et al. Three-fold rotational defects in two-dimensional transition metal dichalcogenides. *Nat. Commun.* **2015**, *6*, 6736.
- (107) Komsa, H.-P.; Krasheninnikov, A. V. Engineering the Electronic Properties of Two-Dimensional Transition Metal Dichalcogenides by Introducing Mirror Twin Boundaries. *Adv. Electron. Mater.* **2017**, *3*, 1600468.
- (108) Vancso, P.; Magda, G. Z.; Peto, J.; Noh, J. Y.; Kim, Y. S.; Hwang, C.; Biro, L. P.; Tapasztó, L. The intrinsic defect structure of exfoliated MoS₂ single layers revealed by scanning tunneling microscopy. *Sci. Rep.* **2016**, *6*, 29726.
- (109) Tumino, F.; Casari, C. S.; Passoni, M.; Russo, V.; Li Bassi, A. Pulsed laser deposition of single-layer MoS₂ on Au(111): from nanosized crystals to large-area films. *Nanoscale Adv.* **2019**, *1*, 643–655.
- (110) Azizi, A.; Zou, X.; Ercius, P.; Zhang, Z.; Elias, A. L.; Perea-Lopez, N.; Stone, G.; Terrones, M.; Yakobson, B. I.; Alem, N. Dislocation motion and grain boundary migration in two-dimensional tungsten disulphide. *Nat. Commun.* **2014**, *5*, 4867.
- (111) Hu, Z. H.; Wu, Z. T.; Han, C.; He, J.; Ni, Z. H.; Chen, W. Two-dimensional transition metal dichalcogenides: interface and defect engineering. *Chem. Soc. Rev.* **2018**, *47*, 3100–3128.
- (112) Schuler, B.; Qiu, D. Y.; Refaely-Abramson, S.; Kastl, C.; Chen, C. T.; Barja, S.; Koch, R. J.; Ogletree, D. F.; Aloni, S.; Schwartzberg, A. M.; et al. Large spin-orbit splitting of deep in-gap defect states of engineered sulfur vacancies in monolayer WS₂. *Phys. Rev. Lett.* **2019**, *123*, No. 076801.
- (113) Zhang, Y.; Zhang, Y. F.; Ji, Q. Q.; Ju, J.; Yuan, H. T.; Ma, D. L.; Liu, M. X.; Chen, Y. B.; Song, X. J.; Hwang, H. Y.; et al. Controlled growth of high-quality monolayer WS₂ layers on sapphire and imaging its grain boundary. *ACS Nano* **2013**, *7*, 8963–8971.
- (114) Rong, Y.; He, K.; Pacios, M.; Robertson, A. W.; Bhaskaran, H.; Warner, J. H. Controlled preferential oxidation of grain boundaries in monolayer tungsten disulfide for direct optical imaging. *ACS Nano* **2015**, *9*, 3695–3703.
- (115) Ly, T. H.; Chiu, M.-H.; Li, M.-Y.; Zhao, J.; Perello, D. J.; Cichocka, M. O.; Oh, H. M.; Chae, S. H.; Jeong, H. Y.; Yao, F.; et al. Observing grain boundaries in CVD-grown monolayer transition metal dichalcogenides. *ACS Nano* **2014**, *8*, 11401–11408.
- (116) Fan, X.; Siris, R.; Hartwig, O.; Duesberg, G. S.; Niklaus, F. Rapid and large-area visualization of grain boundaries in MoS₂ on SiO₂ using vapor hydrofluoric acid. *ACS Appl. Mater. Interfaces* **2020**, *12*, 34049–34057.
- (117) Wang, J. H.; Xu, X. Z.; Qiao, R. X.; Liang, J.; Liu, C.; Zheng, B. H.; Liu, L.; Gao, P.; Jiao, Q. Z.; Yu, D. P.; et al. Visualizing grain boundaries in monolayer MoSe₂ using mild H₂O vapor etching. *Nano Res.* **2018**, *11*, 4082–4089.
- (118) Shehzad, M. A.; Hussain, S.; Lee, J.; Jung, J.; Lee, N.; Kim, G.; Seo, Y. Study of grains and boundaries of molybdenum diselenide and tungsten diselenide using liquid crystal. *Nano Lett.* **2017**, *17*, 1474–1481.
- (119) Jeong, H. Y.; Lee, S. Y.; Ly, T. H.; Han, G. H.; Kim, H.; Nam, H.; Jiong, Z.; Shin, B. G.; Yun, S. J.; Kim, J.; et al. Visualizing point defects in transition-metal dichalcogenides using optical microscopy. *ACS Nano* **2016**, *10*, 770–777.
- (120) Brighty, G. J.; Botham, R. C.; Li, S. H.; Nelson, L.; Mortenson, D. E.; Li, G. C.; Morisseau, C.; Wang, H.; Hammock, B. D.; Sharpless, K. B.; et al. Using sulfuramidimidoyl fluorides that undergo sulfur(VI) fluoride exchange for inverse drug discovery. *Nat. Chem.* **2020**, *12*, 906–913.
- (121) Liu, H.; Grasseschi, D.; Dodda, A.; Fujisawa, K.; Olson, D.; Kahn, E.; Zhang, F.; Zhang, T. Y.; Lei, Y.; Branco, R. B. N.; et al. Spontaneous chemical functionalization via coordination of Au single atoms on monolayer MoS₂. *Sci. Adv.* **2020**, *6*, eabc9308.
- (122) Zheng, J. Y.; Du, H. T.; Jiang, F.; Zhang, Z. M.; Sa, B. S.; He, W. H.; Jiao, L. Y.; Zhan, H. B. Rapid and large-scale quality assessment of two-dimensional MoS₂ using sulfur particles with optical visualization. *Nano Lett.* **2021**, *21*, 1260–1266.
- (123) Yin, X.; Ye, Z.; Chenet, D. A.; Ye, Y.; O'Brien, K.; Hone, J. C.; Zhang, X. Edge nonlinear optics on a MoS₂ atomic monolayer. *Science* **2014**, *344*, 488–490.
- (124) Zhang, X.; Qiao, X. F.; Shi, W.; Wu, J. B.; Jiang, D. S.; Tan, P. H. Phonon and Raman scattering of two-dimensional transition metal dichalcogenides from monolayer, multilayer to bulk material. *Chem. Soc. Rev.* **2015**, *44*, 2757–2785.
- (125) Lu, J.; Liu, H.; Tok, E. S.; Sow, C. H. Interactions between lasers and two-dimensional transition metal dichalcogenides. *Chem. Soc. Rev.* **2016**, *45*, 2494–2515.
- (126) Tebyetekerwa, M.; Zhang, J.; Xu, Z.; Truong, T. N.; Yin, Z.; Lu, Y.; Ramakrishna, S.; Macdonald, D.; Nguyen, H. T. Mechanisms and applications of steady-state photoluminescence spectroscopy in two-dimensional transition-metal dichalcogenides. *ACS Nano* **2020**, *14*, 14579–14604.
- (127) Ferrari, A. C.; Meyer, J. C.; Scardaci, V.; Casiraghi, C.; Lazzeri, M.; Mauri, F.; Piscanec, S.; Jiang, D.; Novoselov, K. S.; Roth, S.; et al. Raman spectrum of graphene and graphene layers. *Phys. Rev. Lett.* **2006**, *97*, 187401.
- (128) Mignuzzi, S.; Pollard, A. J.; Bonini, N.; Brennan, B.; Gilmore, I. S.; Pimenta, M. A.; Richards, D.; Roy, D. Effect of disorder on Raman scattering of single-layer MoS₂. *Phys. Rev. B* **2015**, *91*, 195411.
- (129) Malekpour, H.; Balandin, A. A. Raman-based technique for measuring thermal conductivity of graphene and related materials. *J. Raman Spectrosc.* **2018**, *49*, 106–120.
- (130) Pimenta, M. A.; Del Corro, E.; Carvalho, B. R.; Fantini, C.; Malard, L. M. Comparative study of Raman spectroscopy in graphene and MoS₂-type transition metal dichalcogenides. *Acc. Chem. Res.* **2015**, *48*, 41–47.
- (131) Parkin, W. M.; Balan, A.; Liang, L. B.; Das, P. M.; Lamparski, M.; Naylor, C. H.; Rodriguez-Manzo, J. A.; Johnson, A. T.; Meunier, V.; Drndic, M. Raman shifts in electron-irradiated monolayer MoS₂. *ACS Nano* **2016**, *10*, 4134–4142.
- (132) Li, Y.; Rao, Y.; Mak, K. F.; You, Y.; Wang, S.; Dean, C. R.; Heinz, T. F. Probing symmetry properties of few-layer MoS₂ and h-BN by optical second-harmonic generation. *Nano Lett.* **2013**, *13*, 3329–3333.
- (133) Yin, X. B.; Ye, Z. L.; Chenet, D. A.; Ye, Y.; O'Brien, K.; Hone, J. C.; Zhang, X. Edge nonlinear optics on a MoS₂ atomic monolayer. *Science* **2014**, *344*, 488–490.
- (134) Hsu, W.-T.; Zhao, Z.-A.; Li, L.-J.; Chen, C.-H.; Chiu, M.-H.; Chang, P.-S.; Chou, Y.-C.; Chang, W.-H. Second harmonic generation

from artificially stacked transition metal dichalcogenide twisted bilayers. *ACS Nano* **2014**, *8*, 2951–2958.

(135) Wang, G.; Marie, X.; Gerber, I.; Amand, T.; Lagarde, D.; Bouet, L.; Vidal, M.; Balocchi, A.; Urbaszek, B. Giant enhancement of the optical second-harmonic emission of WSe₂ monolayers by laser excitation at exciton resonances. *Phys. Rev. Lett.* **2015**, *114*, No. 097403.

(136) Cheng, J. X.; Jiang, T.; Ji, Q. Q.; Zhang, Y.; Li, Z. M.; Shan, Y. W.; Zhang, Y. F.; Gong, X. G.; Liu, W. T.; Wu, S. W. Kinetic nature of grain boundary formation in as-grown MoS₂ monolayers. *Adv. Mater.* **2015**, *27*, 4069–4074.

(137) Liu, H.; Li, Y.; You, Y. S.; Ghimire, S.; Heinz, T. F.; Reis, D. A. High-harmonic generation from an atomically thin semiconductor. *Nat. Phys.* **2017**, *13*, 262–265.

(138) Lin, K. I.; Ho, Y. H.; Liu, S. B.; Ciou, J. J.; Huang, B. T.; Chen, C.; Chang, H. C.; Tu, C. L.; Chen, C. H. Atom-dependent edge-enhanced second-harmonic generation on MoS₂ monolayers. *Nano Lett.* **2018**, *18*, 793–797.

(139) Ma, H.; Liang, J.; Hong, H.; Liu, K. H.; Zou, D. X.; Wu, M. H.; Liu, K. H. Rich information on 2D materials revealed by optical second harmonic generation. *Nanoscale* **2020**, *12*, 22891–22903.

(140) Hong, H.; Wu, C. C.; Zhao, Z. X.; Zuo, Y. G.; Wang, J. H.; Liu, C.; Zhang, J.; Wang, F. F.; Feng, J. G.; Shen, H. B.; et al. Giant enhancement of optical nonlinearity in two-dimensional materials by multiphoton-excitation resonance energy transfer from quantum dots. *Nat. Photonics* **2021**, *15*, 510–515.

(141) Wang, G.; Chernikov, A.; Glazov, M. M.; Heinz, T. F.; Marie, X.; Amand, T.; Urbaszek, B. Colloquium: Excitons in atomically thin transition metal dichalcogenides. *Rev. Mod. Phys.* **2018**, *90*, No. 021001.

(142) Lorchat, E.; Lopez, L. E. P.; Robert, C.; Lagarde, D.; Froehlicher, G.; Taniguchi, T.; Watanabe, K.; Marie, X.; Berciaud, S. Filtering the photoluminescence spectra of atomically thin semiconductors with graphene. *Nat. Nanotechnol.* **2020**, *15*, 283–288.

(143) Verhagen, T.; Guerra, V. L. P.; Haider, G.; Kalbac, M.; Vejpravova, J. Towards the evaluation of defects in MoS₂ using cryogenic photoluminescence spectroscopy. *Nanoscale* **2020**, *12*, 3019–3028.

(144) Refaely-Abramson, S.; Qiu, D. Y.; Louie, S. G.; Neaton, J. B. Defect-induced modification of low-lying excitons and valley selectivity in monolayer transition metal dichalcogenides. *Phys. Rev. Lett.* **2018**, *121*, 167402.

(145) Mak, K. F.; He, K.; Lee, C.; Lee, G. H.; Hone, J.; Heinz, T. F.; Shan, J. Tightly bound trions in monolayer MoS₂. *Nat. Mater.* **2013**, *12*, 207–211.

(146) McCreary, K. M.; Hanbicki, A. T.; Sivaram, S. V.; Jonker, B. T. A- and B-exciton photoluminescence intensity ratio as a measure of sample quality for transition metal dichalcogenide monolayers. *APL Mater.* **2018**, *6*, 111106.

(147) Moody, G.; Tran, K.; Lu, X.; Autry, T.; Fraser, J. M.; Mirin, R. P.; Yang, L.; Li, X.; Silverman, K. L. Microsecond valley lifetime of defect-bound excitons in monolayer WSe₂. *Phys. Rev. Lett.* **2018**, *121*, No. 057403.

(148) Zhang, S.; Wang, C. G.; Li, M. Y.; Huang, D.; Li, L. J.; Ji, W.; Wu, S. W. Defect structure of localized excitons in a WSe₂ monolayer. *Phys. Rev. Lett.* **2017**, *119*, No. 046101.

(149) Kioseoglou, G.; Hanbicki, A. T.; Currie, M.; Friedman, A. L.; Gunlycke, D.; Jonker, B. T. Valley polarization and intervalley scattering in monolayer MoS₂. *Appl. Phys. Lett.* **2012**, *101*, 221907.

(150) Demeridou, I.; Papadopoulos, A.; Kourmoulakis, G.; Mouchliadis, L.; Stratakis, E.; Kioseoglou, G. Tuning the valley polarization in WS₂ monolayers via control of active defect sites induced by photochemical doping. *Appl. Phys. Lett.* **2021**, *118*, 123103.

(151) Zou, X. L.; Liu, Y. Y.; Jakobson, B. I. Predicting dislocations and grain boundaries in two-dimensional metal-disulfides from the first principles. *Nano Lett.* **2013**, *13*, 253–258.

(152) Sangwan, V. K.; Hersam, M. C. Electronic transport in two-dimensional materials. *Annu. Rev. Phys. Chem.* **2018**, *69*, 299–325.

(153) Zhu, W. J.; Low, T.; Wang, H.; Ye, P. D.; Duan, X. F. Nanoscale electronic devices based on transition metal dichalcogenides. *2D Mater.* **2019**, *6*, No. 032004.

(154) Mitta, S. B.; Choi, M. S.; Nipane, A.; Ali, F.; Kim, C.; Teherani, J. T.; Hone, J.; Yoo, W. J. Electrical characterization of 2D materials-based field-effect transistors. *2D Mater.* **2021**, *8*, No. 012002.

(155) Liu, Y.; Duan, X. D.; Shin, H.-J.; Park, S.; Huang, Y.; Duan, X. F. Promises and prospects of two-dimensional transistors. *Nature* **2021**, *591*, 43–53.

(156) Ippolito, S.; Kelly, A. G.; Furlan de Oliveira, R.; Stoeckel, M. A.; Iglesias, D.; Roy, A.; Downing, C.; Bian, Z.; Lombardi, L.; Samad, Y. A.; et al. Covalently interconnected transition metal dichalcogenide networks via defect engineering for high-performance electronic devices. *Nat. Nanotechnol.* **2021**, *16*, 592–598.

(157) Fivaz, R.; Mooser, E. Mobility of charge carriers in semiconducting layer structures. *Phys. Rev.* **1967**, *163*, 743–755.

(158) Podzorov, V.; Gershenson, M. E.; Kloc, C.; Zeis, R.; Bucher, E. High-mobility field-effect transistors based on transition metal dichalcogenides. *Appl. Phys. Lett.* **2004**, *84*, 3301–3303.

(159) Kang, K.; Xie, S.; Huang, L. J.; Han, Y.; Huang, P. Y.; Mak, K. F.; Kim, C. J.; Muller, D.; Park, J. High-mobility three-atom-thick semiconducting films with wafer-scale homogeneity. *Nature* **2015**, *520*, 656–660.

(160) Najmaei, S.; Amani, M.; Chin, M. L.; Liu, Z.; Birdwell, A. G.; O'Regan, T. P.; Ajayan, P. M.; Dubey, M.; Lou, J. Electrical transport properties of polycrystalline monolayer molybdenum disulfide. *ACS Nano* **2014**, *8*, 7930–7937.

(161) Wang, D. F.; Yu, H.; Tao, L.; Xiao, W. D.; Fan, P.; Zhang, T. T.; Liao, M. Z.; Guo, W.; Shi, D. X.; Du, S. X.; et al. Bandgap broadening at grain boundaries in single-layer MoS₂. *Nano Res.* **2018**, *11*, 6102–6109.

(162) Wang, Q. Q.; Li, N.; Tang, J.; Zhu, J. Q.; Zhang, Q. H.; Jia, Q.; Lu, Y.; Wei, Z.; Yu, H.; Zhao, Y. C.; et al. Wafer-scale highly oriented monolayer MoS₂ with large domain sizes. *Nano Lett.* **2020**, *20*, 7193–7199.

(163) Li, T. T.; Guo, W.; Ma, L.; Li, W. S.; Yu, Z. H.; Han, Z.; Gao, S.; Liu, L.; Fan, D. X.; Wang, Z. X.; et al. Epitaxial growth of wafer-scale molybdenum disulfide semiconductor single crystals on sapphire. *Nat. Nanotechnol.* **2021**, *16*, 1201–1207.

(164) Yu, Z. H.; Pan, Y. M.; Shen, Y. T.; Wang, Z. L.; Ong, Z. Y.; Xu, T.; Xin, R.; Pan, L. J.; Wang, B. G.; Sun, L. T.; et al. Towards intrinsic charge transport in monolayer molybdenum disulfide by defect and interface engineering. *Nat. Commun.* **2014**, *5*, 5290.

(165) Jadwiszczak, J.; O'Callaghan, C.; Zhou, Y. B.; Fox, D. S.; Weitz, E.; Keane, D.; Cullen, C. P.; O'Reilly, I.; Downing, C.; Shmeliov, A.; et al. Oxide-mediated recovery of field-effect mobility in plasma-treated MoS₂. *Sci. Adv.* **2018**, *4*, eaao5031.

(166) Stanford, M. G.; Pudasaini, P. R.; Gallmeier, E. T.; Cross, N.; Liang, L.; Oyedele, A.; Duscher, G.; Mahjouri-Samani, M.; Wang, K.; Xiao, K.; et al. High conduction hopping behavior induced in transition metal dichalcogenides by percolating defect networks: toward atomically thin circuits. *Adv. Funct. Mater.* **2017**, *27*, 1702829.

(167) Cho, S.; Kim, S.; Kim, J. H.; Zhao, J.; Seok, J.; Keum, D. H.; Baik, J.; Choe, D.-H.; Chang, K. J.; Suenaga, K.; et al. Phase patterning for ohmic homojunction contact in MoTe₂. *Science* **2015**, *349*, 625–627.

(168) Chee, S. S.; Lee, W. J.; Jo, Y. R.; Cho, M. K.; Chun, D.; Baik, H.; Kim, B. J.; Yoon, M. H.; Lee, K.; Ham, M. H. Atomic vacancy control and elemental substitution in a monolayer molybdenum disulfide for high performance optoelectronic device arrays. *Adv. Funct. Mater.* **2020**, *30*, 1908147.

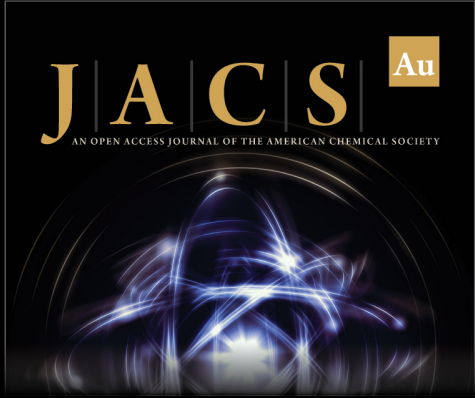
(169) Zhang, X. K.; Liao, Q. L.; Kang, Z.; Liu, B. S.; Liu, X. Z.; Ou, Y.; Xiao, J. K.; Du, J. L.; Liu, Y. H.; Gao, L.; et al. Hidden vacancy benefit in monolayer 2D semiconductors. *Adv. Mater.* **2021**, *33*, 2007051.

(170) Liu, W.; Sarkar, D.; Kang, J.; Cao, W.; Banerjee, K. Impact of contact on the operation and performance of back-gated monolayer MoS₂ field-effect-transistors. *ACS Nano* **2015**, *9*, 7904–7912.


(171) Cui, Y.; Xin, R.; Yu, Z. H.; Pan, Y. M.; Ong, Z.-Y.; Wei, X. X.; Wang, J. Z.; Nan, H. Y.; Ni, Z. H.; Wu, Y.; et al. High-performance monolayer WS_2 field-effect transistors on high-kappa dielectrics. *Adv. Mater.* **2015**, *27*, 5230–5234.


(172) Larentis, S.; Fallahzad, B.; Tutuc, E. Field-effect transistors and intrinsic mobility in ultra-thin MoSe_2 layers. *Appl. Phys. Lett.* **2012**, *101*, 223104.


(173) Sebastian, A.; Pendurthi, R.; Choudhury, T. H.; Redwing, J. M.; Das, S. Benchmarking monolayer MoS_2 and WS_2 field-effect transistors. *Nat. Commun.* **2021**, *12*, 693.



JACS Au
AN OPEN ACCESS JOURNAL OF THE AMERICAN CHEMICAL SOCIETY

 Editor-in-Chief
Prof. Christopher W. Jones
Georgia Institute of Technology, USA

Open for Submissions 

pubs.acs.org/jacsau  ACS Publications
Most Trusted. Most Cited. Most Read.